Final Report

CR 86090

OPTICAL COMMUNICATION AND TRACKING SYSTEMS

By: R. M. DRESSLER E. C. FRASER

Prepared for:

NATIONAL AERONAUTICS AND SPACE ADMINISTRATION
ELECTRONICS RESEARCH CENTER
CAMBRIDGE, MASSACHUSETTS

CONTRACT NAS12-59

STANFORD RESEARCH INSTITUTE

MENLO PARK, CALIFORNIA

STANFORD RESEARCH INSTITUTE
MENLO PARK, CALIFORNIA

October 1967

Final Report

OPTICAL COMMUNICATION AND TRACKING SYSTEMS

Prepared for:

NATIONAL AERONAUTICS AND SPACE ADMINISTRATION
ELECTRONICS RESEARCH CENTER
CAMBRIDGE, MASSACHUSETTS

CONTRACT NAS12-59

By: R. M. DRESSLER E. C. FRASER

SRI Project 5578

Approved: P. E. MERRITT, MANAGER
INFORMATION AND CONTROL LABORATORY

J. D. NOE, EXECUTIVE DIRECTOR
INFORMATION SCIENCE AND ENGINEERING

Copy No. 46

ABSTRACT

The results of research performed by the Information and Control Laboratory of Stanford Research Institute for the Electronics Research Center of the National Aeronautics and Space Administration on Contract NAS12-59 from 1 October 1966 to 30 September 1967 are described in this Final Report. The research program has investigated the control and tracking problems associated with an optical communication system operating between the earth and a spacecraft in the vicinity of Mars. For the system configuration studied, mathematical models of all system components are developed including the relative motion of the two communication terminals, the dynamics of the earth-terminal receiving telescope, the optical propagation properties of the atmosphere and free space, and a statistical description of the optical and mechanical measuring devices used to obtain control or output data from the system.

Two design approaches to this problem are taken. The first, which is based on results from optimal linear estimation and control theory, results in the estimator-controller configuration. The second design employs classical servo theory and yields the autotracker system. The optical communication and tracking system, employing either the estimator-controller or the autotracker, was simulated by means of a digital computer. In addition to assessing the relative performance of these two system designs, computer simulations were also used to evaluate performance sensitivity to such parameters as the magnitude of atmospheric interference and iteration time for the computations.

The simulation tests demonstrate that although, for nominal environmental conditions, both the estimator-controller and the autotracker perform satisfactorily, the estimator-controller is able to maintain satisfactory performance under conditions that render the autotracker unusable.

On the basis of results obtained during this research project, it can be concluded that it is within the capability of present technology to implement a deep-space optical communication system that will provide a significant increase in data rate over presently used techniques.

CONTENTS

ILLUSTRATIONS

TABLES

I INTRODUCTION

As the tasks to be performed by orbital and interplanetary spacecraft become more complex, the communication capacity required between the spacecraft and the earth increases rapidly. For deep-space probes presently being considered, this communication requirement exceeds the capability of present or anticipated RF communication systems. The recent development of lasers, however, makes practical the use of light as the carrier for long-range, high-data-rate communication systems. The extremely narrow beamwidth of lasers permits the concentration of transmitted energy on a distant receiver, while the high frequency of light (10^{14} to 10^{15} Hz) permits very broad-band signal modulation; both are desirable features of a space communication system. In addition to the communication capability of an optical system, the narrow beamwidth permits greatly increased resolution and accuracy in measuring the tracking angles to distant objects. This upgraded tracking data permits real-time orbit determinations that are more accurate than those obtainable via conventional RF tracking techniques, particularly for vehicles near the earth.

The extremely narrow transmitter beamwidths and receiver fields of view (in the order of 0.1 arc second or less) that are necessary to realize efficient operation of an optical communication system dictate that the control systems employed to point the transmitters and receivers be capable of producing an unprecedented level of accuracy and precision. To achieve the required levels of accuracy and precision, the entire system, from concept and configuration to detailed specification of optical, mechanical, and electronic components, must be designed with this high-precision goal in mind. During the past year the Information and Control Laboratory of Stanford Research Institute, under the sponsorship of NASA Electronics Research Center, has been investigating the application of modern control technologies to achieving the tracking accuracy and precision required by an optical communication system. To lend structure to the research project several earth-to-deep

space communication system configurations were considered.[1]* The cooperative system configuration (see Memorandum 8, Sec. II-A), since it appears at present to be the most promising candidate for an actual system design, was selected for further, more detailed study and is described in Sec. II of this report. This included specification of the configuration and establishment of mathematical models for both the earth terminal and the spacecraft terminal of the communication system, as well as a statistical description of the propagation environment and the measurement system. With these specifications, the problem of control system synthesis was undertaken. Due to the atmosphere the earth terminal represents a much more difficult tracking and control problem; hence, primary emphasis was devoted to the design and evaluation of a control system for this terminal. Two approaches were taken to the design of a tracking control system: in Sec. III the results of optimal linear estimation and control theory are applied in the system design; in Sec. IV, for purposes of comparison, an autotracker control system was also synthesized using conventional design techniques. Both of these system designs were simulated by means of a digital computer and their performance compared under similar operational conditions.

This Final Report, covering the year's work, presents the mathematical analyses and the results of the simulation studies performed. The analyses are presented in summary form so as to make this report a complete record of the entire year's project; for the detailed analyses the reader is referred to the technical memoranda and quarterly reports issued during the course of the project. In addition, a complete discussion of the results of the computer simulations is included in Sec. V.

The computer program that was developed on this project, together with the complete documentation according to NASA specifications, has been forwarded to the Electronics Research Center. This program simulates the operation of the estimator-controller configuration, which is

---

*References are listed at the end of the report.

described in Sec. III, and a conventional autotracker, which is described in Sec. IV, within an optical communication and tracking system.

II SYSTEM CONFIGURATION

A. Spacecraft Terminal

The control of the spacecraft terminal entails two distinct functions: (1) tracking of the signal incoming from earth to maintain correct alignment of the spacecraft receiving telescope, and (2) offsetting of the transmitter axis from the receiver axis to compensate for the relative motion of the earth and the spacecraft during the roundtrip transit time of the optical signal. Considering the second, and simpler, of these two functions, it has been stated that the maximum angular offset (point-ahead angle) required between the transmitter and receiver axis is less than 30 to 50 arc seconds.[1] This being the case, the same telescope would be used for both receiver and transmitter, the angular offset being obtained by effectively displacing the transmitter relative to the receiver in the focal plane of the telescope. (Although this is effectively what is done, the actual implementation of this offset would undoubtedly be accomplished by a system of beam steerers inserted between the transmitter and the optics used to combine the transmitter and receiver beams.) Since this relative displacement is a purely deterministic function (see Memorandum 8, Sec. III-A) that is periodically updated from the earth, the only equipment required to implement the transmitter offset is a mechanism for real-time evaluation of the offset function and an instrument servo for adjusting the beam steerers to realize this offset angle. Thus, except for the periodic updating of the offset function, the pointing of the transmitter is accomplished "open loop." Furthermore, since the transmitter is pointed with respect to the receiver rather than with respect to some arbitrary reference frame, conventional instrument servo technology is sufficient to provide the offset accuracies required (on the order of 0.1 percent).

The receiver, on the other hand, must perform a tracking function so as to maintain the signal from the earth terminal within its field of view--and ideally, located on its optical axis. To accomplish this task,

the receiver tracking system must be able to track any angular variations arising from: relative terminal motion; transmission medium effects; attitude changes of the spacecraft due to crew motion, equipment motion, meteorite impacts, and solar pressures; thermally-induced distortions of the telescope structure; and any small oscillations due to excitation of structural resonances.

Considering these in the order in which they are introduced, the pointing angles from the spacecraft to the earth change due to the motion of both the earth and the spacecraft. These motions, however, give rise to slowly varying angular changes. The only transmission medium effects between the two terminals are those introduced by the earth's atmosphere. The net contribution of the atmosphere is to deviate the earth transmitter's beam away from its nominal direction. If the transmitted beam is wide enough to ensure continuous spacecraft illumination, then this beam deviation will not be discernable at the spacecraft receiver, and will not enter into receiver performance.

Attitude changes of the spacecraft will appear as target motion that must be tracked by the spacecraft receiver. Equipment or crew motion and meteorite impacts can be modeled as impulsive torques applied to a pure inertia, resulting in a constant rate of change of spacecraft attitude.[2] Solar pressure acting on any spacecraft assymetry will exert a constant torque, and thus will induce a constant acceleration of spacecraft attitude. This latter acceleration is very small and will contribute spacecraft attitude changes that are very small compared to those from other sources. It is assumed that the spacecraft itself is attitude-stabilized by means of reaction jets, control moment gyros, or other means, such that the spacecraft attitude is held to within some limits of a nominal attitude. (An overall spacecraft attitude stability of one degree, for example, is presently considered routine.) Thus the receiver tracking will have to compensate for any deviation of the spacecraft from its nominal attitude. Since such attitude changes are the result of torques acting on a pure inertia, they will be slowly varying in nature. Present estimates are that the attitude-stabilization system for a spacecraft carrying a large telescope and a crew will have a

natural frequency no greater than 3 rad/sec (0.48 Hz)[2,3]--a figure indicative of the smoothness of the attitude disturbances expected.

Thermal distortions of the telescope structure, resulting from differential heating of the telescope parts by solar radiation, will cause the optical axis to deviate from the nominal mechanical axis. To maintain optical contact, the receiver tracking system must compensate for this deviation. However, the rate of change of this distortion will be very slow since, except during maneuvers, the spacecraft will maintain essentially a constant attitude with respect to the sun.

By far the most difficult tracking task for the receiver system is compensating for the telescope structural resonances. These small amplitude oscillations of structural members will cause small but rapid excursions of the telescope optical axis about its nominal pointing direction. (Present estimates indicate significant distortions at rates up to 21 Hz.)[2] For continuous, small field-of-view pointing, these pointing angle variations must be compensated for by the receiver tracking system.

From the above description of sources of pointing disturbances, it appears that a two-loop receiver tracking system will be required onboard the spacecraft. The primary loop of this system is a low frequency mechanical system that orients the entire telescope with respect to the attitude-stablized spacecraft. This loop would accomplish the gross tracking of the target motion with respect to the spacecraft, and compensation for gross errors such as spacecraft attitude errors and thermally-induced distortions. In addition to the mechanical tracking capability, a small-angle, high-speed tracking system will be required to accommodate the small amplitude, high-frequency disturbances such as the structural resonances of the telescope and its supports. This system can be implemented by means of high-speed beam steerers[1] inserted within the optical system of the telescope.

The input data for both the high-speed and the mechanical tracking systems will be obtained from an optical pointing error detector. The accuracy with which tracking can be accomplished by a conventional tracking system is limited only by the accuracy of the error detector. (This

statement is true only in those cases where no data readout is required, and the only task is maintaining the optical axis aligned with the incoming signal, and where the tracking system is fast enough to compensate for any disturbances with negligible dynamic error. Since both of these conditions are satisfied in this application, the statement is appropriate.) In Memorandum 9[4] a technique has been developed for obtaining angular pointing errors that are extremely accurate and virtually noise-free--the standard deviation of the angular measurement is at least several orders of magnitude smaller than the measurement itself.

Considering the facts that the spacecraft receiver tracking system is required only to maintain optical-system alignment--no data output is needed--and that the determination of the direction of the incoming signal can be made virtually noise free, it can be concluded that a conventional autotracker control system will produce satisfactory tracking system performance. The estimator-controller configuration proposed for the earth terminal will not be needed since an accurate estimate of the earth's position is not required--at least within the context of the communication and tracking system--and the input signal direction is not subjected to a large disturbance as is the case for a receiver looking directly through the atmosphere. Since the technology of conventional autotrack systems is already well developed, and their capabilities well known, it is not considered appropriate within the scope of this project to perform either a detailed analysis or simulation of the on-board telescope tracking system, but rather to simply establish that a conventional tracking-system design will be adequate.

B. Earth Terminal

The control of the earth terminal consists of the same two basic functions as required of the spacecraft terminal: (1) tracking of the incoming signal from the spacecraft to maintain correct alignment of the earth-based receiving telescope, and (2) offsetting of the transmitter axis from the receiver axis to compensate for the relative motion of the earth and the spacecraft during the round-trip transit time of the optical signal. The second of these functions can be accomplished

in the same manner as described in Sec. II-A. The tracking function, however, is made more difficult by fluctuations in the signal's angle-of-arrival introduced by the earth's atmosphere. Since these fluctuations are of a magnitude and frequency spectrum that is outside the capabilities of a conventional autotracker system, the more sophisticated estimator-controller system configuration shown in Fig. 1 has been proposed.

In order to study this system in detail, it is necessary to develop mathematical models for each of the elements in the system. The specific derivations of these models are presented in Memorandum 9[4] and, therefore, only a summary of these results is presented in this report.

The geometric angle of arrival of the incoming optical signal that is to be tracked by the earth-based receiver is determined by the relative motion of the spacecraft with respect to the tracking site. The geometry of the problem is shown in Fig. 2. The 1_s and 2_s axes, which lie in the plane of the ecliptic (the plane of the earth's orbit), and the 3_s axis, which is perpendicular to this plane, define a sun-centered Cartesian coordinate system (the 1_s axis is taken to be the winter solstice).

1. Spacecraft

A model to describe the spacecraft motion is taken to be

$$\ddot{x}_{1_s} = -\frac{\mu_s x_{1_s}}{r_s^3}$$

$$\ddot{x}_{2_s} = -\frac{\mu_s x_{2_s}}{r_s^3}$$

$$\ddot{x}_{3_s} = -\frac{\mu_s x_{3_s}}{r_s^3} \qquad (1)$$

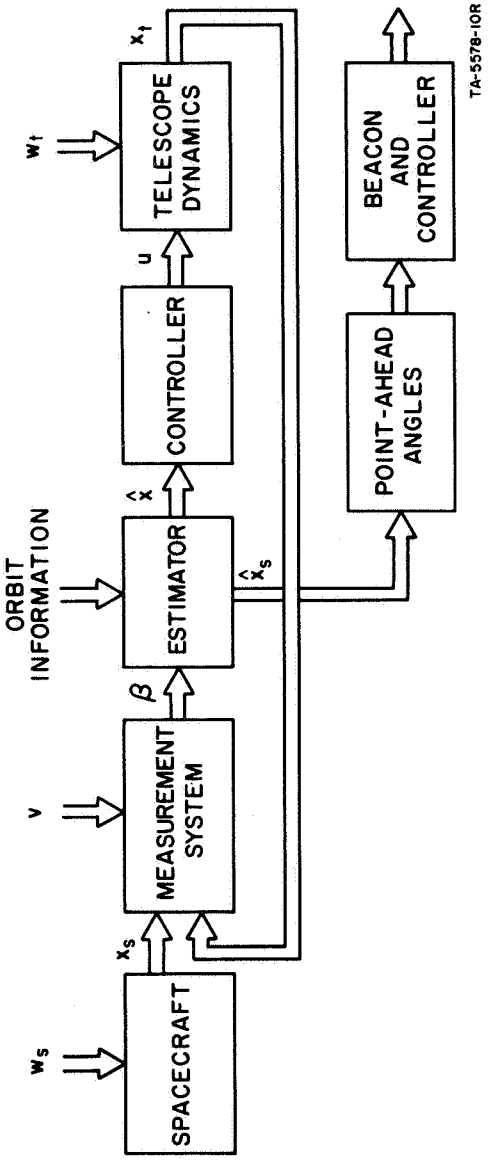

FIG. 1 STRUCTURE OF EARTH TERMINAL

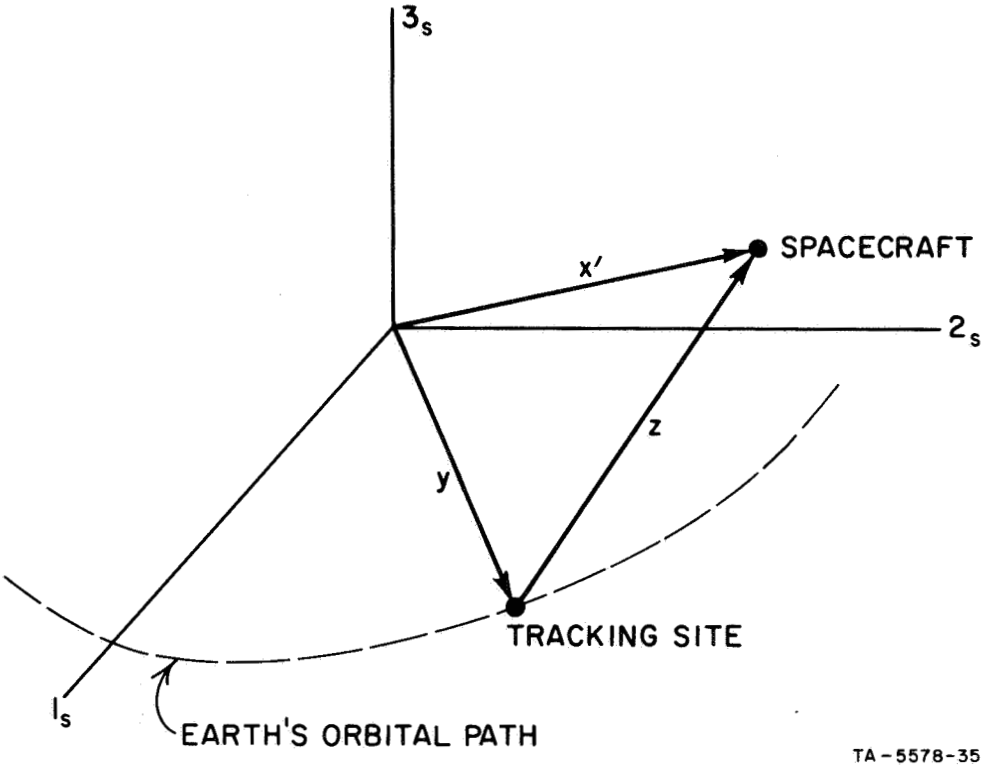

FIG. 2 RELATIVE MOTION OF SPACECRAFT AND TRACKING SITE

where

$$r_s = \left(x_{1_s}^2 + x_{2_s}^2 + x_{3_s}^2 \right)^{\frac{1}{2}}$$

μ_s = the product of the universal gravitational constant and the mass of the sun

$= 1.3255 \times 10^{20}\ m^3/sec^2$

$x_{1_s}, x_{2_s}, x_{3_s}$ = the position coordinates of the spacecraft with respect to the 1_s, 2_s, 3_s coordinate system.

This mathematical model assumes that the spacecraft is on an interplanetary trajectory and that the only force acting upon it is the sun's gravitational attraction. If the spacecraft were in a planetary orbit,

the model would have to be modified accordingly. It should be noted that the differential equations (1) merely give an approximate description of the spacecraft motion, but are sufficient as a model for the purposes of applying optimal estimation and control theory to the system design (see Sec. III).

The equations of motion (1) can be put into state-variable form upon definition of the six-dimensional state vector of the spacecraft,

$$x_s = \begin{bmatrix} x_{1_s} \\ x_{2_s} \\ x_{3_s} \\ \dot{x}_{1_s} \\ \dot{x}_{2_s} \\ \dot{x}_{3_s} \end{bmatrix} , \tag{2}$$

which enables the differential equations (1) to be rewritten concisely as

$$\dot{x}_s = \begin{bmatrix} \dot{x}_{1_s} \\ \dot{x}_{2_s} \\ \dot{x}_{3_s} \\ -\dfrac{\mu_s x_{1_s}}{r_s^3} \\ -\dfrac{\mu_s x_{2_s}}{r_s^3} \\ -\dfrac{\mu_s x_{3_s}}{r_s^3} \end{bmatrix} = f_s(x_s) \tag{3}$$

where $f_s(x_s)$ is a six-dimensional vector function of the state x_s.

In order to account for actual input disturbances as well as inaccuracies in the mathematical model of spacecraft motion, a random forcing term is included in Eq. (3), as follows:

$$\dot{x}_s = f_s(x_s) + w_s \tag{4}$$

where the six-dimensional vector w_s (having elements w_{i_s}) is assumed to be a white, Gaussian noise process with zero mean and covariance Q_s.

The actual trajectory of the spacecraft (i.e., the trajectory to be tracked by the telescope in the digital-computer simulation) is generated by a set of differential equations that are more complete than the model described in Eqs. (1). For an Earth-Mars mission, the forces acting upon the spacecraft due to the gravitational fields of Mars and the earth, as well as the sun, are considered. Hence, the actual equations of motion for the spacecraft are taken to be

$$\ddot{x}_{1_s} = -\frac{\mu_s x_{1_s}}{r_s^3} - \frac{\mu_m\left(x_{1_s} - x_{1_m}\right)}{r_m^3} - \frac{\mu_e\left(x_{1_s} - x_{1_e}\right)}{r_e^3}$$

$$\ddot{x}_{2_s} = -\frac{\mu_s x_{2_s}}{r_s^3} - \frac{\mu_m\left(x_{2_s} - x_{2_m}\right)}{r_m^3} - \frac{\mu_e\left(x_{2_s} - x_{2_e}\right)}{r_e^3}$$

$$\ddot{x}_{3_s} = -\frac{\mu_s x_{3_s}}{r_s^3} - \frac{\mu_m\left(x_{3_s} - x_{3_m}\right)}{r_m^3} - \frac{\mu_e\left(x_{3_s} - x_{3_e}\right)}{r_e^3} \tag{5}$$

where

$$r_m = \left[\left(x_{1_s} - x_{1_m}\right)^2 + \left(x_{2_s} - x_{2_m}\right)^2 + \left(x_{3_s} - x_{3_m}\right)^2\right]^{\frac{1}{2}}$$

$$r_e = \left[\left(x_{1_s} - x_{1_e}\right)^2 + \left(x_{2_s} - x_{2_e}\right)^2 + \left(x_{3_s} - x_{3_e}\right)^2\right]^{\frac{1}{2}}$$

μ_m = the product of the universal gravitational constant and the mass of Mars

$= 4.251 \times 10^{13}\ m^3/sec^2$

μ_e = the product of the universal gravitational constant and the mass of the earth

$= 3.986 \times 10^{14}\ m^3/sec^2$

$x_{1_m}, x_{2_m}, x_{3_m}$ = the position coordinates of Mars in the 1_s, 2_s, 3_s coordinate system

$x_{1_e}, x_{2_e}, x_{3_e}$ = the position coordinates of the earth in the 1_s, 2_s, 3_s coordinate system.

It should be noted that the x_{i_m} and x_{i_e} are well-known functions of time dictated by the orbital motions of Mars and the earth, respectively.

2. Telescope Dynamics

To describe the telescope's mechanical motion a very simplified diagram of its structure, relative to the 1_t, 2_t, 3_t coordinate system of the tracking site, is given in Fig. 3. The 1_t and 2_t axes define a plane parallel to the earth's equatorial plane, with the 1_t axis defined as lying in the plane of the great circle passing through the tracking site and the earth's poles (the 1_t axis is determined by the tracking site's longitude, which is related to the prime meridian by a constant angle); the 3_t axis is parallel to the earth's polar axis. It has been assumed that the telescope operates on an equatorial mount; hence, tracking and pointing are in terms of the telescope declination and hour angles,* φ_t and θ_t. The telescope tube is gimbal-mounted on the telescope support and rotates about the declination axis in a plane perpendicular to the plane determined by the 1_t and 2_t axes; the entire

*This terminology is consistent with that used in astronomy.

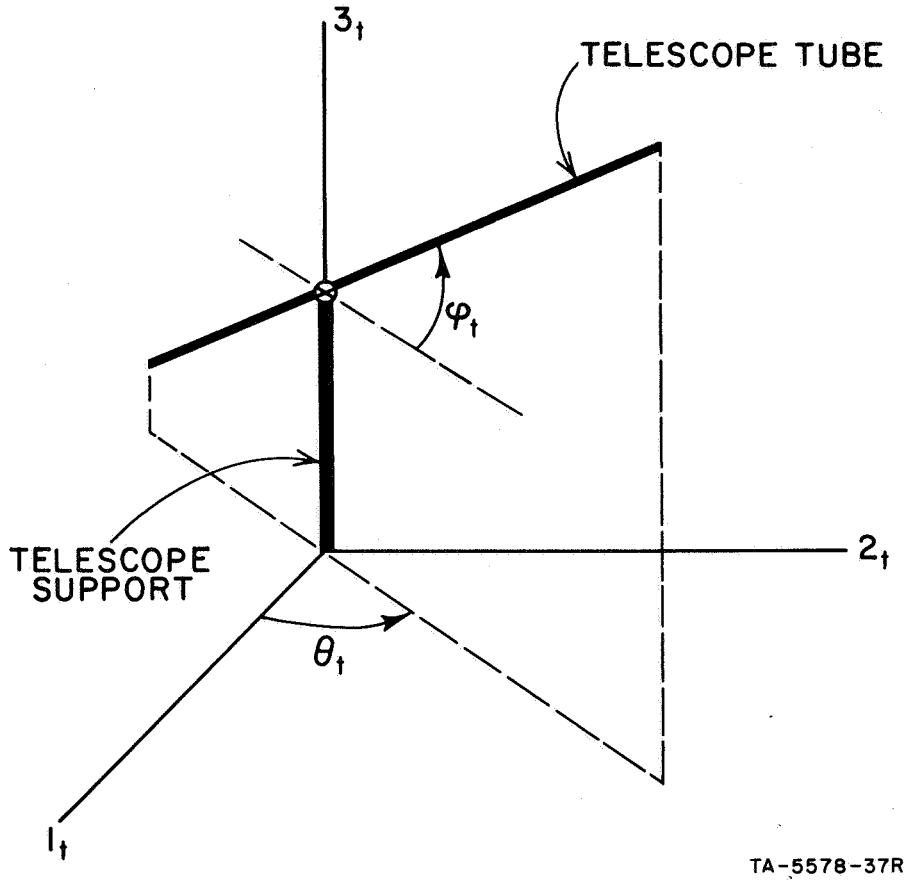

FIG. 3 MECHANICAL STRUCTURE OF TELESCOPE

telescope structure rotates about the polar (or hour-angle) axis, which corresponds to the 3_t axis. The polar axis subtends an angle of $90^\circ - \psi_t$ with a normal to the earth at the tracking site, where ψ_t is the latitude of the site. The relative orientation of the 1_t, 2_t, 3_t and 1_s, 2_s, 3_s coordinate systems is given by the orthogonal transformation

$$T_{t/s} = \begin{bmatrix} \cos\eta \cos(\Omega t + \delta) & \sin(\Omega t + \delta) & -\sin\eta \cos(\Omega t + \delta) \\ -\cos\eta \sin(\Omega t + \delta) & \cos(\Omega t + \delta) & \sin\eta \sin(\Omega t + \delta) \\ \sin\eta & 0 & \cos\eta \end{bmatrix} \quad (6)$$

where

Ω = angular rate of rotation of earth

= 7.28×10^{-5} rad/sec

δ = arbitrary angle

η = angle between earth's polar axis and a normal to the plane of the ecliptic

= 23.45° (0.41 rad).

A linear model to describe the mechanical behavior of the telescope and its drive motors is taken to be

$$J_{\varphi} \ddot{\varphi}_t + f_{\varphi} \dot{\varphi}_t = u_{\varphi}$$

$$J_{\theta}(t) \ddot{\theta}_t + f_{\theta} \dot{\theta}_t = u_{\theta} \qquad (7)$$

where

J_{φ} = moment of inertia of the telescope tube about the declination axis

$J_{\theta}(t) = J'_{\theta} + J_{\varphi} \cos^2 \varphi_t$

= instantaneous moment of inertia of the entire telescope structure about the polar axis

J'_{θ} = moment of inertia about the polar axis of the telescope structure with the telescope tube oriented at $\varphi_t = 90^{\circ}$

f_{φ}, f_{θ} = damping factors due to the bearings that support the telescope's declination and polar axes, respectively

u_{φ}, u_{θ} = motor torques about the telescope's declination and polar axes, respectively; these quantities correspond to the control variables.

In modeling the telescope's mechanical motion, bending of the telescope structure caused by the force of gravity is not included. Since this

bending (which is essentially a static effect) can be determined experimentally as a function of the angles φ_t and θ_t, it can be compensated for in the system design and need not be included in the telescope's dynamic equations. For deep-space communication (e.g., an Earth-Mars mission), the telescope will be subjected to very small angular rates and accelerations. Thus, since the telescope is an extremely rigid structure, it is reasonable to assume that any bending of the telescope structure due to these accelerations is negligible. Therefore, in the above mathematical model it has been assumed that the telescope tube and support are both perfectly rigid. Thermal distortion of the telescope is essentially a steady-state effect (having a time constant on the order of hours) which can readily be measured and compensated for in the system. Hence it is not necessary to include this effect in the telescope's dynamic equations. Additionally, J_θ can be considered to be a function of time. It should be noted that the differential equations (7) merely give an approximate description of the telescope's mechanical motion and its drive motors, but are sufficient as a model for the purposes of applying optimal estimation and control theory to the system design (see Sec. III).

It is assumed that hydrostatic bearings are used to support the telescope mount's declination and polar axes. Hydrostatic bearings are employed to obtain a high degree of smoothness in the mechanical motion of the telescope and, hence, to permit the development of a high-precision pointing and tracking system. Furthermore, these bearings reduce the friction to exceedingly small values, so that the telescope can be driven by relatively small motors for the low tracking rates that are required. With hydrostatic bearings, the breakaway torque (static friction) is negligible, and it is not necessary to include this effect in the model for the telescope's dynamics. It is also assumed that direct-drive torque motors are employed to generate the torques (controls) u_φ and u_θ, which drive the telescope about the declination and polar axes, respectively. Torque motors are designed to provide very smooth output torque (independent of shaft position), thus making possible a high degree of resolution in position at low operating

speeds. Direct-drive torque motors are attached directly to the load itself (i.e., the telescope shafts); hence, there is no gear train required, with its inherent windup and backlash errors. Furthermore, the dynamics of the drive motors (having time constants less than one millisecond) are considerably faster than the telescope's dynamic behavior and are considered as having a transfer function of unity in the above model.

It is assumed that the earth-based terminal is equipped with a 120-inch (approximately 3-meter) telescope, similar in structure to the Lick Observatory telescope on Mt. Hamilton in California. The specifications for this telescope[5] have been used to arrive at the following nominal values for the telescope parameters defined in Eq. (7):

$$J_{\varphi} = 1.9 \times 10^{6} \ \text{kg}\cdot\text{m}^2$$

$$J'_{\theta} = 0.6 \times 10^{6} \ \text{kg}\cdot\text{m}^2$$

$$f_{\varphi} = 0.8 \times 10^{5} \ \frac{\text{N}\cdot\text{m}}{\text{rad/sec}}$$

$$f_{\theta} = 3.1 \times 10^{5} \ \frac{\text{N}\cdot\text{m}}{\text{rad/sec}} \quad . \tag{8}$$

The equations of motion (7) can be put into state-variable form by defining the four-dimensional state vector of the telescope

$$x_t = \begin{bmatrix} \varphi_t \\ \dot{\varphi}_t \\ \theta_t \\ \dot{\theta}_t \end{bmatrix} \tag{9}$$

and the two-dimensional control vector

$$u = \begin{bmatrix} u_\varphi \\ u_\theta \end{bmatrix} , \tag{10}$$

which enables the differential equations (7) to be rewritten concisely as

$$\begin{aligned} \dot{x}_t &= F_t(t)\, x_t + D_t(t)\, u \\ &= \begin{bmatrix} F_\varphi & 0 \\ 0 & F_\theta(t) \end{bmatrix} x_t + \begin{bmatrix} D_\varphi & 0 \\ 0 & D_\theta(t) \end{bmatrix} u \end{aligned} \tag{11}$$

where

$$F_\varphi = \begin{bmatrix} 0 & 1 \\ 0 & -\frac{f_\varphi}{J_\varphi} \end{bmatrix} \qquad F_\theta(t) = \begin{bmatrix} 0 & 1 \\ 0 & -\frac{f_\theta}{J_\theta(t)} \end{bmatrix}$$

$$D_\varphi = \begin{bmatrix} 0 \\ \frac{1}{J_\varphi} \end{bmatrix} \qquad D_\theta(t) = \begin{bmatrix} 0 \\ \frac{1}{J_\theta(t)} \end{bmatrix} .$$

Equation (11) indicates the uncoupled behavior of the telescope's declination and polar channels. This model permits the computation of the optimal control law to be greatly simplified, as will be shown in Sec. III-B.

Since a digital computer is to be employed for the purpose of controlling the telescope, the differential equation (11) will be converted into an equivalent difference equation. This is accomplished by assuming that u, as well as F_θ and D_θ, is constant over the interval $[k\Delta t, (k + 1)\Delta t]$:

$$x_t(k+1) = \Phi_t(k)\, x_t(k) + \Delta_t(k)\, u(k)$$

$$= \begin{bmatrix} \Phi_\varphi & 0 \\ 0 & \Phi_\theta(k) \end{bmatrix} x_t(k) + \begin{bmatrix} \Delta_\varphi & 0 \\ 0 & \Delta_\theta(k) \end{bmatrix} u(k) \qquad (12)$$

where

$$\Phi_\varphi = \sum_{i=0}^{\infty} \frac{F_\varphi^i \cdot (\Delta t)^i}{i!}$$

$$\Phi_\theta(k) = \sum_{i=0}^{\infty} \frac{F_\theta^i(k) \cdot (\Delta t)^i}{i!}$$

$$\Delta_\varphi = \left[\sum_{i=0}^{\infty} \frac{F_\varphi^i \cdot (\Delta t)^{i+1}}{(i+1)!} \right] D_\varphi$$

$$\Delta_\theta(k) = \left[\sum_{i=0}^{\infty} \frac{F_\theta^i(k) \cdot (\Delta t)^{i+1}}{(i+1)!} \right] D_\theta(k) \qquad (13)$$

where $x_t(k)$ and $u(k)$ are abbreviated representations for $x_t(k\Delta t)$ and $u(k\Delta t)$, respectively (Δt is the iteration interval). The matrices Φ_t and Δ_t can be computed with an arbitrary degree of accuracy by taking a suitably large, but finite, number of terms in the series expansions of Eqs. (13).

In order to account for actual input disturbances as well as inaccuracies in the mathematical model of the mechanical behavior of the telescope and its drive motors, a random forcing term is included in Eq. (12) as follows:

$$x_t(k+1) = \Phi_t(k)\, x_t(k) + \Delta_t(k)\, u(k) + w_t(k) \qquad (14)$$

where the four-dimensional vector w_t (having elements w_{i_t}) is assumed to be a white, Gaussian noise process with zero mean and covariance Q_t. It is also assumed that the telescope is enclosed in a dome so that it is not subjected to wind disturbances, but such load disturbances can easily be included in this formulation.

The actual mechanical behavior of the telescope and its drive motors (i.e., the telescope's mechanical motion in the digital computer simulation) is generated by a set of differential equations that are more complete than the model described in Eqs. (7). The actual equations of motion for the telescope and its drive motors are taken to be

$$J_\varphi \ddot{\varphi}_t + f_\varphi \dot{\varphi}_t + J_\varphi \dot{\theta}_t^2 \cos \varphi_t \sin \varphi_t = u_\varphi$$

$$\left(J'_\theta + J_\varphi \cos^2 \varphi_t\right) \ddot{\theta}_t + f_\theta \dot{\theta}_t - 2J_\varphi \dot{\theta}_t \dot{\varphi}_t \cos \varphi_t \sin \varphi_t = u_\theta \quad . \quad (15)$$

The nonlinear terms in the above differential equations are introduced by the motion of the telescope about its declination and polar axes. For very small tracking rates these nonlinear terms will be negligible.

3. Measurement System

The measurement system consists of the following elements.

Digital Angular Readouts: These are employed to measure φ_t and θ_t, the angular positions of the telescope's declination and polar (or hour-angle) axes, respectively. These observations are corrupted by the measurement noises v_{φ_t} and v_{θ_t}, which are modeled as white, Gaussian noise processes with zero means and variances denoted by $\sigma^2_{\varphi_t}$ and $\sigma^2_{\theta_t}$. (Actually, these measurement noises have discrete probability densities.) In addition, v_{φ_t} and v_{θ_t} are statistically independent.

Optical Detector: This measures the angular pointing errors, $\varphi_0 - \varphi'_s$ and $\theta_0 - \theta'_s$, where φ_0 and θ_0 are the declination and hour angles of the telescope's optical axis, respectively, and φ'_s and θ'_s are the declination and hour angles of the optical signal from the spacecraft. The terms defining the instantaneous angle of arrival of the signal are

given by $\varphi_s' = \varphi_s + v_{\varphi_a}$ and $\theta_s' = \theta_s + v_{\theta_a}$, where φ_s and θ_s are the spacecraft's declination and hour angles, respectively (these angles, which determine the geometric angle of arrival of the signal to be tracked, are functions of x_s and will be defined below), and v_{φ_a} and v_{θ_a} represent the effect of atmospheric-induced image excursion, which is a relatively rapid refractive bending of the optical beam (it is not necessary to include the effect of the steady-state refraction, since it can be accurately measured and compensated for in the system design). The random disturbances v_{φ_a} and v_{θ_a} can be modeled as white,* Gaussian noise processes with zero means and variances given by $\sigma^2_{\varphi_a}$ and $\sigma^2_{\theta_a}$. Additionally, v_{φ_a} and v_{θ_a} are assumed to be statistically independent. It is assumed that a charge-storage tube (such as an iconoscope or an image orthicon) employing a raster scan is used as the optical detector; in a tracking mode, the pointing errors are small enough so that the operation of the detector can be considered linear. Other detection techniques, such as a tetrahedral beam-splitting prism or conical scanning, could also be employed. The observations of the angular pointing errors are corrupted by the measurement noises v_{φ_d} and v_{θ_d}, which can be modeled as white, Gaussian noise processes with zero means and variances denoted by $\sigma^2_{\varphi_d}$ and $\sigma^2_{\theta_d}$. Furthermore, v_{φ_d} and v_{θ_d} are uncorrelated.

Coherent Code Transponder on Spacecraft: This is employed to measure the spacecraft range ρ_s (this quantity, which is a function of x_s, will be defined below). This measurement can be obtained by use of the primary optical channel or an auxiliary microwave link. The observation of the spacecraft range is corrupted by the measurement noise v_ρ, which is modeled as a white, Gaussian noise process with zero mean and variance given by σ^2_ρ.

---

*For the purposes of estimation this is a reasonable approximation, since the power spectral densities of v_{φ_a} and v_{θ_a} have bandwidths of about 250 rad/sec, which is appreciably greater than the bandwidth of the telescope's mechanical motion (0.05 to 0.50 rad/sec).

The development of the above mathematical models for the statistics of the measurement system are presented in greater detail in Ref. 4.

The spacecraft's declination and hour angles, φ_s and θ_s, are defined in the same way as the corresponding telescope angles, which are shown in Fig. 3. The expressions for φ_s and θ_s are obtained as follows: In the 1_s, 2_s, 3_s coordinate system (see Fig. 2), the three-dimensional vector defining the geometric line of sight from the tracking site to the spacecraft is given by

$$z_s = x_s' - y_s \tag{16}$$

where

$$x_s' = \begin{bmatrix} x_{1_s} \\ x_{2_s} \\ x_{3_s} \end{bmatrix} = \text{the spacecraft position}$$

and y_s, which is the position of the earth-based tracking site, is the sum of two components: the earth's orbital motion and the earth's rotation about its axis--both of which are well-known functions of time. Using the orthogonal transformation of Eq. (6), z_s can be expressed in the 1_t, 2_t, 3_t coordinate system as

$$z_t = T_{t/s}\, z_s \quad . \tag{17}$$

Then it can be shown that

$$\varphi_s = \sin^{-1}\left[\frac{z_{3_t}}{\left(z_{1_t}^2 + z_{2_t}^2 + z_{3_t}^2\right)^{\frac{1}{2}}}\right] \tag{18}$$

and

$$\theta_s = \sin^{-1}\left[\frac{z_{2_t}}{\left(z_{1_t}^2 + z_{2_t}^2\right)^{\frac{1}{2}}}\right] \quad . \tag{19}$$

The spacecraft range ρ_s, which is the distance from the tracking site to the spacecraft, is given by

$$\rho_s = |z_t| = |z_s| \quad . \tag{20}$$

By substituting from Eqs. (16) and (17), one can express φ_s, θ_s, and ρ_s in terms of the x_{i_s}, which are contained in the spacecraft state vector [Eq. (2)], and the elements of y_s, which are known time-varying functions describing the earth's orbital and rotational motion.

The system described in Fig. 1 consists of two tracking loops operating in series. The telescope's mechanical axis and its drive motors are located in the primary tracking loop, together with the estimator and controller. The function of the primary loop is to provide smooth tracking of φ_s and θ_s, the slowly varying mean value of the incoming signal's angle of arrival, by the telescope's mechanical axis, which is defined by φ_t and θ_t. By providing smooth tracking of the angle-of-arrival mean value, the signal's instantaneous angle of arrival (defined by $\varphi_s + v_{\varphi_a}$ and $\theta_s + v_{\theta_a}$) will be kept within the dynamic range of the beam steerer, which is in the secondary loop. The secondary tracking loop is a direct feedback of the optical detector output to a small-angle, high-frequency beam steerer. The purpose of this secondary tracking loop is to cause the telescope's optical axis (defined by φ_0 and θ_0) to follow the rapid fluctuations in the signal's angle of arrival, thus ensuring the maximum possible signal-to-noise ratio. This is achieved by nulling the angular pointing errors.

The tracking configuration for the declination channel is shown in Fig. 4; the polar (or hour-angle) channel has the identical form. It

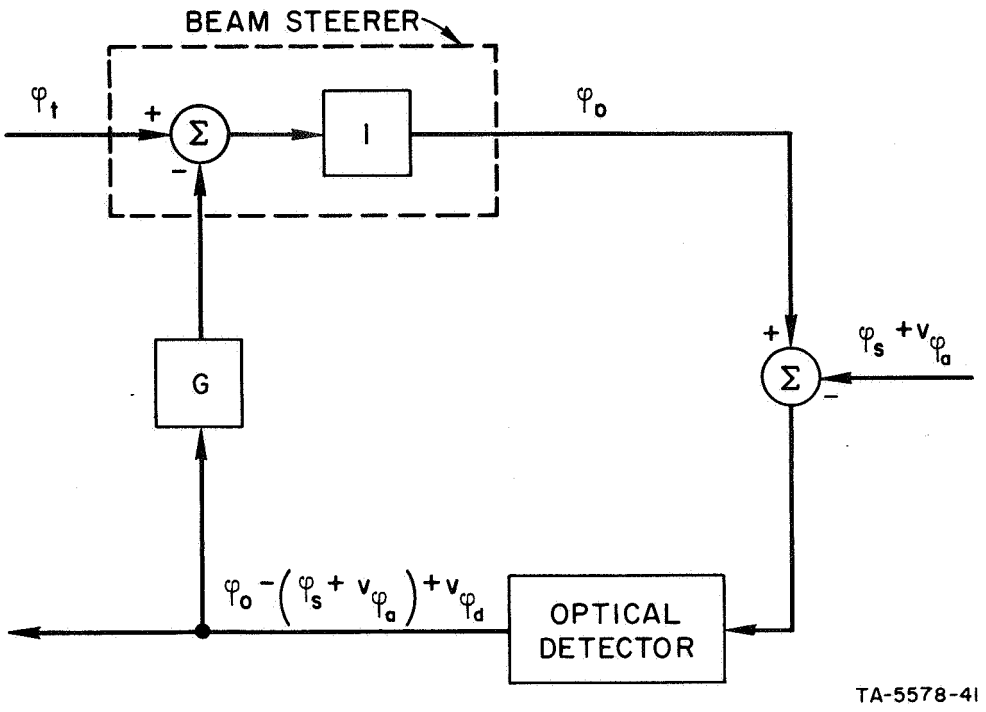

FIG. 4 TRACKING CONFIGURATION (declination channel)

is assumed that the beam steerer is implemented by a system of piezoelectrically-rotated mirrors, which provide orthogonal deflections of the optical beam about the declination and polar axes. This type of beam steerer can be designed to have a bandwidth of about 20 to 50 kHz, and be essentially linear over a dynamic range of ±100 seconds of arc. Since the beam steerer has a bandwidth that is considerably greater than the bandwidth of the telescope's mechanical motion, it is reasonable to consider it to be described by a transfer function of unity. The feedback gain G (where $G > 0$) is chosen sufficiently large, consistent with stability considerations, to reduce the angular pointing error to an acceptable level.

From Fig. 4, it can be shown that the output of the optical detector for the declination channel is given by

$$\varphi_0 - \left(\varphi_s + v_{\varphi_a}\right) + v_{\varphi_d} = \frac{1}{1+G}\left[\varphi_t - \left(\varphi_s + v_{\varphi_a}\right) + v_{\varphi_d}\right] \quad . \quad (21)$$

Similarly, the output of the optical detector for the polar channel is

$$\theta_0 - \left(\theta_s + v_{\theta_a}\right) + v_{\theta_d} = \frac{1}{1+G}\left[\theta_t - \left(\theta_s + v_{\theta_a}\right) + v_{\theta_d}\right] \quad . \quad (22)$$

The equations for the measurement system can be expressed concisely by defining the 10-dimensional state vector x of the overall system, which consists of the spacecraft state x_s and the telescope state x_t:

$$x = \begin{bmatrix} x_s \\ \\ x_t \end{bmatrix} \quad . \quad (23)$$

Hence, the measurement equations can be defined in terms of the state vector x by the five-dimensional measurement vector

$$\beta(k) = \begin{bmatrix} \varphi_t(k) - \varphi_s(k) \\ \theta_t(k) - \theta_s(k) \\ \rho_s(k) \\ \varphi_t(k) \\ \theta_t(k) \end{bmatrix} + \begin{bmatrix} v_{\varphi_d}(k) - v_{\varphi_a}(k) \\ v_{\theta_d}(k) - v_{\theta_a}(k) \\ v_\rho(k) \\ v_{\varphi_t}(k) \\ v_{\theta_t}(k) \end{bmatrix} = h[x(k), k] + v(k) \quad . \quad (24)$$

From Eqs. (18), (19), and (20), the spacecraft's declination and hour angles and the spacecraft range are time-varying, nonlinear functions of the system state--$\varphi_s[x(k), k]$, $\theta_s[x(k), k]$, and $\rho_s[x(k), k]$. Hence, the measurement equations are time-varying and nonlinear as represented by $h[x(k), k]$. From the above discussion, the five-dimensional measurement noise vector v(k) is a white, Gaussian noise process with

$$E[v(k)] = 0$$

$$E[v(k)\ v^T(k)] = R(k) = \begin{bmatrix} \sigma^2_{\varphi_d}(k) + \sigma^2_{\varphi_a}(k) & & & & \\ & \sigma^2_{\theta_d}(k) + \sigma^2_{\theta_a}(k) & & & \\ & & \sigma^2_{\rho}(k) & & \\ & & & \sigma^2_{\varphi_t}(k) & \\ & & & & \sigma^2_{\theta_t}(k) \end{bmatrix} . \tag{25}$$

The covariance matrix R(k) takes this form since the optical-detector noise, the noise introduced by image excursion, the noise on the range measurement, and the digital angular-readout noise are mutually independent. For the assumed system parameters,[2] the variances in R(k) are given as follows:

$$\sigma^2_{\varphi_d}(k) = \sigma^2_{\theta_d}(k) = 6 \times 10^{-19}\ \text{rad}^2$$

$$\sigma^2_{\varphi_a}(k) = \sigma^2_{\theta_a}(k) = 2.25 \times 10^{-10}\ \text{rad}^2$$

$$\sigma^2_{\rho}(k) = 10^8\ \text{m}^2$$

$$\sigma^2_{\varphi_t}(k) = \sigma^2_{\theta_t}(k) = 2.25 \times 10^{-12}\ \text{rad}^2 \quad . \tag{26}$$

III ESTIMATOR-CONTROLLER CONFIGURATION

The function of the estimator is to generate a "best" estimate of the present system state x, based on all measurements β (which are corrupted by noise) up to the present time. This estimate is then employed in the controller to compute a "best" control u with respect to a given performance criterion. The estimation and control equations are derived in Secs. III-A and III-B, respectively. The approach taken assumes that the equations for the estimator and the controller can be solved separately. Since the optical-tracking problem is nonlinear, this assumption may yield a solution that is not strictly optimal.[6] However, this approach yields a solution that is both computationally feasible and, as shown by the results of extensive computer simulations (see Sec. V), yields excellent performance.

A. Estimation Equations

In this section the equations for the estimator are developed by employing the extended Kalman filter. This concept is an application to nonlinear systems of work done by Kalman[7] in linear estimation theory, in which the estimate obtained at each time is the maximum likelihood estimate conditioned on all measurements up to that time. Justification for this approach and a derivation of the extended (or linearized) Kalman filter is presented in Memorandum 6[8] and, hence, will not be repeated here.

From Eqs. (4) and (14), the random disturbance in the model of the overall system is given by the ten-dimensional vector

$$w(k) = \begin{bmatrix} w_s(k) \\ \\ w_t(k) \end{bmatrix} ,$$

which is a white, Gaussian noise process with

$$E[w(k)] = 0$$

$$E[w(k)\ w^T(k)] = Q(k) = \begin{bmatrix} Q_s(k) & 0 \\ 0 & Q_t(k) \end{bmatrix} \quad . \qquad (27)$$

A model for the measurement noise v(k) is given in Eqs. (25). The initial state x(0) is taken to be a Gaussian random variable with

$$E[x(0)] = \hat{x}(0/0)$$

$$E[\{x(0) - \hat{x}(0/0)\}\ \{x(0) - \hat{x}(0/0)\}^T] = P(0/0) \quad . \qquad (28)$$

Furthermore, it is assumed that w(k), v(k), and x(0) are uncorrelated.

The resulting estimation equations can be considered as consisting of two parts: prediction and correction (or regression). The following notation will be employed:

$$\hat{x}(i/j) \triangleq E[x(i)/\beta(j),\ldots,\beta(1),u(j-1),\ldots,u(0)] \quad ,$$

$$P(i/j) \triangleq E[\{x(i) - \hat{x}(i/j)\}\{x(i) - \hat{x}(i/j)\}^T/\beta(j),\ldots,\beta(1),u(j-1),\ldots,u(0)] \quad .$$

These expectations are conditioned on the previous measurements and controls.

1. Prediction

Given the estimate of the system state at the k^{th} instant $[\hat{x}(k/k)]$ and the assumption that $E[w(k)] = 0$, the predicted system state for the $k+1^{th}$ instant $[\hat{x}(k+1/k)]$ is obtained from Eqs. (4) and (14):*

*The nonlinear differential equation for x_s may be integrated by a more accurate method if necessary.

$$\hat{x}(k+1/k) = \begin{bmatrix} \hat{x}_s(k+1/k) \\ \hat{x}_t(k+1/k) \end{bmatrix} = \begin{bmatrix} \hat{x}_s(k/k) + f_s[\hat{x}_s(k/k)]\Delta t \\ \Phi_t(k)\ \hat{x}_t(k/k) + \Delta_t(k)\ u(k) \end{bmatrix} \quad . \quad (29)$$

The covariance of the error in this prediction is given by

$$P(k+1/k) = \Phi(k)\ P(k/k)\ \Phi^T(k) + Q(k) \quad (30)$$

where

$$\Phi(k) = \begin{bmatrix} \Phi_s(k) & 0 \\ 0 & \Phi_t(k) \end{bmatrix} \quad (31)$$

with $\Phi_t(k)$ defined in Eq. (12) and $\Phi_s(k)$ obtained from the nonlinear differential equation (3) by linearization about the estimate $\hat{x}(k/k)$ [or $\hat{x}_s(k/k)$]; i.e.,

$$\Phi_s(k) = I + \frac{\partial f_s}{\partial x_s}\,[\hat{x}_s(k/k)]\ \Delta t \quad (32)$$

in which

$$\frac{\partial f_s}{\partial x_s} = \begin{bmatrix} 0 & 0 & 0 & 1 & 0 & 0 \\ 0 & 0 & 0 & 0 & 1 & 0 \\ 0 & 0 & 0 & 0 & 0 & 1 \\ \dfrac{\mu_s\left(2x_{1_s}^2 - x_{2_s}^2 - x_{3_s}^2\right)}{r_s^5} & \dfrac{3\mu_s x_{1_s} x_{2_s}}{r_s^5} & \dfrac{3\mu_s x_{1_s} x_{3_s}}{r_s^5} & 0 & 0 & 0 \\ \dfrac{3\mu_s x_{2_s} x_{1_s}}{r_s^5} & \dfrac{\mu_s\left(2x_{2_s}^2 - x_{1_s}^2 - x_{3_s}^2\right)}{r_s^5} & \dfrac{3\mu_s x_{2_s} x_{3_s}}{r_s^5} & 0 & 0 & 0 \\ \dfrac{3\mu_s x_{3_s} x_{1_s}}{r_s^5} & \dfrac{3\mu_s x_{3_s} x_{2_s}}{r_s^5} & \dfrac{\mu_s\left(2x_{3_s}^2 - x_{1_s}^2 - x_{2_s}^2\right)}{r_s^5} & 0 & 0 & 0 \end{bmatrix}$$

2. Correction

The prediction $\hat{x}(k + 1/k)$ is then corrected by using the actual measurement at the $k + 1^{th}$ instant $[\beta(k + 1)]$ and the predicted measurement for the $k + 1^{th}$ instant $[\hat{\beta}(k + 1/k)]$, which is obtained from Eq. (24) by substituting $\hat{x}(k + 1/k)$ and using the assumption that $E[v(k + 1)] = 0$:

$$\hat{\beta}(k + 1/k) = h[\hat{x}(k + 1/k),\ k + 1] \quad . \tag{33}$$

Hence, the estimate of the system state at the $k + 1^{th}$ instant is given by

$$\hat{x}(k+1/k+1) = \begin{bmatrix} \hat{x}_s(k+1/k+1) \\ \\ \hat{x}_t(k+1/k+1) \end{bmatrix} = \hat{x}(k+1/k) + W(k+1)\ [\beta(k+1) - \hat{\beta}(k+1/k)] \tag{34}$$

where the 10×5 weighting matrix is given by

$$W(k+1) = P(k+1/k)\ H^T(k+1)\ [R(k+1) + H(k+1)\ P(k+1/k)\ H^T(k+1)]^{-1} \quad , \tag{35}$$

and $H(k + 1)$ is obtained from Eq. (24) by linearization about the prediction $\hat{x}(k + 1/k)$ [or $\hat{x}_s(k + 1/k)$]; i.e.,

$$H(k + 1) = H[\hat{x}(k + 1/k),\ k + 1] = \frac{\partial h}{\partial x}\ [\hat{x}(k + 1/k),\ k + 1] \tag{36}$$

in which

$$\frac{\partial h}{\partial x} = \begin{bmatrix} a_1 & a_2 & a_3 & 0 & 0 & 0 & 1 & 0 & 0 & 0 \\ b_1 & b_2 & b_3 & 0 & 0 & 0 & 0 & 0 & 1 & 0 \\ c_1 & c_2 & c_3 & 0 & 0 & 0 & 0 & 0 & 0 & 0 \\ 0 & 0 & 0 & 0 & 0 & 0 & 1 & 0 & 0 & 0 \\ 0 & 0 & 0 & 0 & 0 & 0 & 0 & 0 & 1 & 0 \end{bmatrix}$$

with

$$a_i = -\frac{\partial \varphi_s}{\partial x_{i_s}} \quad , \quad b_i = -\frac{\partial \theta_s}{\partial x_{i_s}} \quad , \quad \text{and} \quad c_i = \frac{\partial \rho_s}{\partial x_{i_s}} \quad .$$

Applying the chain rule for differentiation to Eqs. (16) to (19), it can be shown that the a_i and b_i are given by

$$\begin{bmatrix} a_1 \\ a_2 \\ a_3 \end{bmatrix} = -T^T_{t/s} \begin{bmatrix} \partial \varphi_s / \partial z_{1_t} \\ \partial \varphi_s / \partial z_{2_t} \\ \partial \varphi_s / \partial z_{3_t} \end{bmatrix} \tag{37}$$

where

$$\frac{\partial \varphi_s}{\partial z_{1_t}} = \frac{-z_{1_t} z_{3_t}}{\left(z^2_{1_t} + z^2_{2_t}\right)^{\frac{1}{2}} |z_t|^2}$$

$$\frac{\partial \varphi_s}{\partial z_{2_t}} = \frac{-z_{2_t} z_{3_t}}{\left(z^2_{1_t} + z^2_{2_t}\right)^{\frac{1}{2}} |z_t|^2}$$

$$\frac{\partial \varphi_s}{\partial z_{3_t}} = \frac{\left(z^2_{1_t} + z^2_{2_t}\right)^{\frac{1}{2}}}{|z_t|^2} \quad ,$$

and

$$\begin{bmatrix} b_1 \\ b_2 \\ b_3 \end{bmatrix} = -T^T_{t/s} \begin{bmatrix} \partial \theta_s / \partial z_{1_t} \\ \partial \theta_s / \partial z_{2_t} \\ \partial \theta_s / \partial z_{3_t} \end{bmatrix} \tag{38}$$

where

$$\frac{\partial \theta_s}{\partial z_{1_t}} = \frac{-z_{2_t}}{z_{1_t}^2 + z_{2_t}^2}$$

$$\frac{\partial \theta_s}{\partial z_{2_t}} = \frac{z_{1_t}}{z_{1_t}^2 + z_{2_t}^2}$$

$$\frac{\partial \theta_s}{\partial z_{3_t}} = 0 \quad .$$

The $\partial \varphi_s / \partial z_{j_t}$ and $\partial \theta_s / \partial z_{j_t}$ can be rewritten in terms of the x_{i_s} and the elements of y by substitution from Eqs. (16) and (17).

From Eq. (20), it is a straightforward matter to show that the c_i are given by

$$c_i = \frac{x_{i_s} - y_{i_s}}{\left[\sum_{j=1}^{3} \left(x_{j_s} - y_{j_s}\right)^2\right]^{\frac{1}{2}}} \quad . \tag{39}$$

The covariance of the error in the estimate $\hat{x}(k + 1/k + 1)$ is

$$P(k+1/k+1) = [I - W(k+1)H(k+1)]P(k+1/k)$$

$$= P(k+1/k) - P(k+1/k)H^T(k+1)[R(k+1) + H(k+1)P(k+1/k)H^T(k+1)]^{-1}$$

$$\cdot H(k+1)P(k+1/k) \quad . \tag{40}$$

The extended Kalman filter [Eqs. (29), (30), (34), (35), and (40)] can be readily implemented on a digital computer. The a priori state estimate $\hat{x}(0/0)$ and its error covariance $P(0/0)$ are used to initialize these recursive equations. It should be noted that in the extended Kalman filter, the nonlinear equations (3) and (22) are used in Eqs. (29) and (34) to obtain the predicted state and the predicted measurement. The

linearization of Eqs. (3) and (22), in order to obtain Φ_s and H, is only employed to calculate the covariance matrices P and the weighting matrix W.

Since the overall system is nonlinear, the above solution to the estimation problem is suboptimal. The extent to which this solution to the estimation problem differs from the optimum is mainly dependent upon the accuracy of the linearization of Eq. (3), the differential equation for x_s, and of Eq. (22), the measurement equation.

However, as shown in Sec. V, the estimator derived in this manner is capable of achieving an excellent level of performance.

B. Control Equations

1. General

In this section the control problem is solved by application of optimal linear control theory. Consider the performance criterion

$$J = E\left[\sum_{k=0}^{N}\left\{[\varphi_t(k) - \varphi_s(k)]^2 + [\theta_t(k) - \theta_s(k)]^2 + [b_\varphi u_\varphi^2(k) + b_\theta u_\theta^2(k)]\right\}\right]. \tag{41}$$

The cost associated with control (where $b_\varphi, b_\theta \geq 0$) is essential in order to guarantee that u_φ and u_θ (the motor torques) do not become too large, which, in turn, would cause the telescope rates to exceed their permissible ranges of values. However, the actual tracking performance is given by the first two terms in Eq. (41).

For the purpose of deriving a control law, it will be assumed that

$$\ddot{\varphi}_s = \ddot{\theta}_s = 0 \quad . \tag{42}$$

This is a very reasonable assumption for a deep-space tracking problem, and enables the dynamics of the spacecraft angles to be modeled as

$$\begin{bmatrix} \varphi_s(k+1) \\ \dot{\varphi}_s(k+1) \end{bmatrix} = \Phi_d \begin{bmatrix} \varphi_s(k) \\ \dot{\varphi}_s(k) \end{bmatrix} \tag{43}$$

and

$$\begin{bmatrix} \theta_s(k+1) \\ \dot{\theta}_s(k+1) \end{bmatrix} = \Phi_h \begin{bmatrix} \theta_s(k) \\ \dot{\theta}_s(k) \end{bmatrix} \quad , \tag{44}$$

where

$$\Phi_d = \Phi_h = \begin{bmatrix} 1 & \Delta t \\ 0 & 1 \end{bmatrix} \quad .$$

If necessary, higher-order models can be used to describe the dynamics of the spacecraft angles.

The quantities $\dot{\varphi}_s$ and $\dot{\theta}_s$ are obtained from Eqs. (18) and (19):

$$\dot{\varphi}_s = \sum_{j=1}^{3} \frac{\partial \varphi_s}{\partial z_{j_t}} \dot{z}_{j_t} \tag{45}$$

and

$$\dot{\theta}_s = \sum_{j=1}^{3} \frac{\partial \theta_s}{\partial z_{j_t}} \dot{z}_{j_t} \quad , \tag{46}$$

where the partial derivatives of φ_s and θ_s are given in Eqs. (37) and (38), respectively, and the terms $\dot{z}_{j_t}$ are obtained from Eqs. (16) and (17) as

$$\dot{z}_t = T_{t/s}\, \dot{z}_s + \dot{T}_{t/s}\, z_s \tag{47}$$

in which

$$\dot{z}_s = \dot{x}'_s - \dot{y}_s$$

$$\dot{x}'_s = \begin{bmatrix} \dot{x}_{1_s} \\ \dot{x}_{2_s} \\ \dot{x}_{3_s} \end{bmatrix}$$

and $\dot{y}_s$ is a well-known function of time, determined by the earth's orbital motion and the earth's rotation about its axis. By substituting from Eqs. (37), (38), and (47), $\dot{\varphi}_s$ and $\dot{\theta}_s$ can be expressed in terms of the x_{i_s} and $\dot{x}_{i_s}$, which are contained in the spacecraft state vector [Eq. (2)], and the elements of y_s and $\dot{y}_s$

The state of the system can be defined by the 8-dimensional vector

$$\underline{x} = \begin{bmatrix} \varphi_s \\ \dot{\varphi}_s \\ \theta_s \\ \dot{\theta}_s \\ x_t \end{bmatrix} , \tag{48}$$

in which the telescope state x_t is defined in Eq. (9). The equations of motion for $\underline{x}$ are given by

$$\underline{x}(k+1) = \underline{\Phi}(k)\ \underline{x}(k) + \underline{\Delta}(k)\ u(k) \quad , \tag{49}$$

where

$$\underline{\Phi}(k) = \begin{bmatrix} \Phi_1 & 0 \\ 0 & \Phi_t(k) \end{bmatrix}$$

$$\Phi_1 = \begin{bmatrix} \Phi_d & 0 \\ 0 & \Phi_h \end{bmatrix}$$

$$\underline{\Delta}(k) = \begin{bmatrix} 0 \\ \\ \Delta_t(k) \end{bmatrix} \quad ,$$

and the matrices $\Phi_t(k)$ and $\Delta_t(k)$ are defined in Eq. (12).

Rewriting J of Eq. (41) in vector-matrix form, gives

$$J = E\left[\sum_{k=0}^{N} \{\underline{x}^T(k)\ A\ \underline{x}(k) + u^T(k)\ B\ u(k)\}\right] \tag{50}$$

where

$$B = \begin{bmatrix} b_\varphi & 0 \\ \\ 0 & b_\theta \end{bmatrix}$$

$$A = \begin{bmatrix} A_1 & A_3 \\ \\ A_3^T & A_2 \end{bmatrix} \quad ,$$

in which A is symmetric and positive semidefinite. It is a straightforward matter to determine A:

$$A_1 = A_2 = \begin{bmatrix} 1 & & \bigcirc \\ & 0 & \\ \bigcirc & & 1 \\ & & & 0 \end{bmatrix}$$

$$A_3 = \begin{bmatrix} -1 & & \bigcirc \\ & 0 & \\ \bigcirc & & -1 \\ & & & 0 \end{bmatrix} \quad .$$

The design objective is to find the sequence of controls

$$u(0),\ u(1),\ \ldots,\ u(N)$$

that minimizes J. The control equations will be derived by applying some results, obtained by Larson, which are described in Quarterly Report 3;[9] this work is an extension of results in optimal linear control theory.

The optimal control is given by

$$u(k) = \begin{bmatrix} u_{\varphi}(k) \\ \\ u_{\theta}(k) \end{bmatrix} = - K(k)\ \underline{\hat{x}}(k/k) \tag{51}$$

where the 2 × 8 gain matrix is given by

$$K(k) = \left[B + \underline{\Delta}^T(k)\ P_c(k+1)\ \underline{\Delta}^T(k)\right]^{-1}\ \underline{\Delta}^T(k)\ P_c(k+1)\ \underline{\Phi}(k) \tag{52}$$

and the 8 × 8 matrix P_c satisfies the discrete Riccati equation

$$\begin{aligned} P_c(k) &= A + \underline{\Phi}^T(k)\ P_c(k+1)\ \underline{\Phi}(k) \\ &\quad - \underline{\Phi}^T(k)\ P_c(k+1)\ \underline{\Delta}(k) \left[B + \underline{\Delta}^T(k)\ P_c(k+1)\ \underline{\Delta}(k)\right]^{-1} \\ &\quad \cdot \underline{\Delta}^T(k)\ P_c(k+1)\ \underline{\Phi}(k) \qquad 0 \le k < N \quad , \end{aligned} \tag{53}$$

$$P_c(N) = A \quad .$$

For convenience, $P_c(k)$ will be rewritten in a form entirely analogous to A:

$$P_c(k) = \begin{bmatrix} P_1(k) & P_3(k) \\ \\ P_3^T(k) & P_2(k) \end{bmatrix}$$

where $P_c(k)$ is symmetric and positive semidefinite. Upon performance of the indicated matrix multiplications, the optimal control in Eq. (51) becomes

$$u(k) = -\left[B + \Delta_t^T(k)\, P_2(k+1)\, \Delta_t(k)\right]^{-1} \Delta_t^T(k)\, P_3^T(k+1)\, \Phi_1\, \hat{\Psi}(k/k)$$
$$-\left[B + \Delta_t^T(k)\, P_2(k+1)\, \Delta_t(k)\right]^{-1} \Delta_t^T(k)\, P_2(k+1)\, \Phi_t(k)\, \hat{x}_t(k/k) \quad (54)$$

where

$$\hat{\Psi}(k/k) = \begin{bmatrix} \hat{\varphi}_s(k/k) \\ \hat{\dot{\varphi}}_s(k/k) \\ \hat{\theta}_s(k/k) \\ \hat{\dot{\theta}}_s(k/k) \end{bmatrix} \quad (55)$$

and the term $\hat{x}_t(k/k)$ is the estimate of the telescope state. The estimates in Eq. (55) are obtained from Eqs. (18), (19), (45), and (46); i.e.,

$$\begin{aligned} \hat{\varphi}_s(k/k) &= \varphi_s[\hat{x}_s(k/k),\, k] \\ \hat{\theta}_s(k/k) &= \theta_s[\hat{x}_s(k/k),\, k] \\ \hat{\dot{\varphi}}_s(k/k) &= \dot{\varphi}_s[\hat{x}_s(k/k),\, k] \\ \hat{\dot{\theta}}_s(k/k) &= \dot{\theta}_s[\hat{x}_s(k/k),\, k] \end{aligned} \quad (56)$$

where $\hat{x}_s(k/k)$ is the estimate of the spacecraft state. It should be noted that since Eqs. (18), (19), (45), and (46) are nonlinear functions of x_s, the estimates given in Eq. (56) are not optimal in the usual sense.

The Riccati equation (53) can be partitioned into separate equations for P_1, P_2, and P_3:

$$P_1(k) = A_1 + \Phi_1^T P_1(k+1)\Phi_1$$
$$- \Phi_1^T P_3^T(k+1)\,\Delta_t(k)\left[B + \Delta_t^T(k)P_2(k+1)\Delta_t(k)\right]^{-1}\Delta_t^T(k)P_3(k+1)\Phi_1$$
$$0 \le k < N \quad , \tag{57}$$

$$P_1(N) = A_1 \quad ;$$

$$P_2(k) = A_2 + \Phi_t^T(k)P_2(k+1)\Phi_t(k)$$
$$- \Phi_t^T(k)P_2(k+1)\Delta_t(k)\left[B + \Delta_t^T(k)P_2(k+1)\Delta_t(k)\right]^{-1}\Delta_t^T(k)P_2(k+1)\Phi_t(k)$$
$$0 \le k < N \quad , \tag{58}$$

$$P_2(N) = A_2 \quad ;$$

and

$$P_3(k) = A_3 + \Phi_1^T P_3(k+1)\,\Phi_t(k)$$
$$- \Phi_1^T P_3(k+1)\,\Delta_t(k)\left[B + \Delta_t^T(k)P_2(k+1)\Delta_t(k)\right]^{-1}\Delta_t^T(k)P_2(k+1)\Phi_t(k)$$
$$0 \le k < N \quad , \tag{59}$$

$$P_3(N) = A_3 \quad .$$

Equation (58) can be solved for the 4 × 4 matrix P_2 independently of Eqs. (57) and (59). It is interesting to note that Eq. (58) is the Riccati equation for the system of Eq. (14), with the performance criterion

$$E\left[\sum_{k=0}^{N}\left\{x_t^T(k)\,A_2 x_t(k) + u^T(k)\,Bu(k)\right\}\right] \quad ;$$

the optimal control for the problem is given by the second term in Eq. (54). Once P_2 has been found, it is substituted into Eq. (59), which is a linear equation in the 4 × 4 matrix P_3. Since the 4 × 4 matrix P_1 does not enter into the control equation (54) or the calculation of P_2 and P_3, it is not necessary to solve Eq. (57).

From the form of $\Phi_t(k)$ and $\Delta_t(k)$, which are defined in Eq. (12), and A_2, which is defined in Eq. (50), it can be shown that the solution to Eq. (58) is of the form

$$P_2(k) = \begin{bmatrix} P_\varphi(k) & 0 \\ 0 & P_\theta(k) \end{bmatrix} . \tag{60}$$

This simplification permits the Riccati equation (58) to be partitioned into separate equations for the 2 × 2 matrices P_φ and P_θ:

$$\begin{aligned} P_\varphi(k) &= A_\varphi + \Phi_\varphi^T P_\varphi(k+1)\Phi_\varphi \\ &\quad - \Phi_\varphi^T P_\varphi(k+1)\Delta_\varphi\left[b_\varphi + \Delta_\varphi^T P_\varphi(k+1)\Delta_\varphi\right]^{-1}\Delta_\varphi^T P_\varphi(k+1)\Phi_\varphi \\ &\qquad\qquad 0 \le k < N \quad , \\ P_\varphi(N) &= A_\varphi = \begin{bmatrix} 1 & 0 \\ 0 & 0 \end{bmatrix} ; \end{aligned} \tag{61}$$

and

$$\begin{aligned} P_\theta(k) &= A_\theta + \Phi_\theta^T(k) P_\theta(k+1)\Phi_\theta(k) \\ &\quad - \Phi_\theta^T(k) P_\theta(k+1)\Delta_\theta(k)\left[b_\theta + \Delta_\theta^T(k) P_\theta(k+1)\Delta_\theta(k)\right]^{-1}\Delta_\theta^T(k) P_\theta(k+1)\Phi_\theta(k) \\ &\qquad\qquad 0 \le k < N \quad , \\ P_\theta(N) &= A_\theta = \begin{bmatrix} 1 & 0 \\ 0 & 0 \end{bmatrix} . \end{aligned} \tag{62}$$

From the form of Φ_1, which is defined in Eq. (49), A_3, which is defined in Eq. (50), $P_2(k)$, which is given in Eq. (50), $\Phi_t(k)$, and $\Delta_t(k)$, it can be shown that the solution to Eq. (59) is of the form

$$P_3(k) = \begin{bmatrix} P_{3\varphi}(k) & 0 \\ 0 & P_{3\theta}(k) \end{bmatrix} . \tag{63}$$

This simplification permits Eq. (59) to be partitioned into separate equations for the 2×2 matrices $P_{3\varphi}$ and $P_{3\theta}$:

$$\begin{aligned} P_{3\varphi}(k) &= A_{3\varphi} + \Phi_d^T P_{3\varphi}(k+1)\Phi_\varphi \\ &\quad - \Phi_d^T P_{3\varphi}(k+1)\Delta_\varphi \left[b_\varphi + \Delta_\varphi^T P_\varphi(k+1)\Delta_\varphi \right]^{-1} \Delta_\varphi^T P_\varphi(k+1)\Phi_\varphi \\ &\qquad\qquad 0 \le k < N \quad , \end{aligned} \tag{64}$$

$$P_{3\varphi}(N) = A_{3\varphi} = \begin{bmatrix} -1 & 0 \\ 0 & 0 \end{bmatrix} ;$$

and

$$\begin{aligned} P_{3\theta}(k) &= A_{3\theta} + \Phi_h^T P_{3\theta}(k+1)\Phi_\theta(k) \\ &\quad - \Phi_h^T P_{3\theta}(k+1)\dot{\Delta}_\theta(k) \left[b_\theta + \Delta_\theta^T(k) P_\theta(k+1)\Delta_\theta(k) \right]^{-1} \Delta_\theta^T(k) P_\theta(k+1)\Phi_\theta(k) \\ &\qquad\qquad 0 \le k < N , \end{aligned} \tag{65}$$

$$P_{3\theta}(N) = A_{3\theta} = \begin{bmatrix} -1 & 0 \\ 0 & 0 \end{bmatrix} .$$

Finally, the two components of the control u(k) can be obtained separately as

$$u_\varphi(k) = -\left[b_\varphi + \Delta_\varphi^T P_\varphi(k+1)\,\Delta_\varphi\right]^{-1} \Delta_\varphi^T P_{3\varphi}^T(k+1)\,\Phi_d \begin{bmatrix} \hat{\varphi}_s(k/k) \\ \hat{\dot{\varphi}}_s(k/k) \end{bmatrix}$$

$$-\left[b_\varphi + \Delta_\varphi^T P_\varphi(k+1)\,\Delta_\varphi\right]^{-1} \Delta_\varphi^T P_\varphi(k+1)\,\Phi_\varphi\,\hat{x}_\varphi(k/k) \qquad (66)$$

and

$$u_\theta(k) = -\left[b_\theta + \Delta_\theta^T(k)\,P_\theta(k+1)\,\Delta_\theta(k)\right]^{-1} \Delta_\theta^T(k)\,P_{3\theta}^T(k+1)\Phi_h \begin{bmatrix} \hat{\theta}_s(k/k) \\ \hat{\dot{\theta}}_s(k/k) \end{bmatrix}$$

$$-\left[b_\theta + \Delta_\theta^T(k)\,P_\theta(k+1)\,\Delta_\theta(k)\right]^{-1} \Delta_\theta^T(k)\,P_\theta(k+1)\Phi_\theta(k)\,\hat{x}_\theta(k/k)\ , \qquad (67)$$

where

$$\hat{x}_\varphi(k/k) = \begin{bmatrix} \hat{\varphi}_t(k/k) \\ \hat{\dot{\varphi}}_t(k/k) \end{bmatrix} \qquad \hat{x}_\theta(k/k) = \begin{bmatrix} \hat{\theta}_t(k/k) \\ \hat{\dot{\theta}}_t(k/k) \end{bmatrix}\ .$$

Thus, the computational requirements have been reduced markedly. Instead of solving the 8×8 Riccati equation (53) for P_c, we may perform the following steps: first solve the 2×2 Riccati equations (61) and (62) for P_φ and P_θ; then, using P_φ and P_θ, calculate $P_{3\varphi}$ and $P_{3\theta}$ from the 2×2 linear equations (64) and (65). The optimal control u is then obtained by substituting these matrices, together with the state estimate $\hat{x}(k/k)$ [$\hat{\varphi}_s(k/k)$, $\hat{\theta}_s(k/k)$, $\hat{\dot{\varphi}}_s(k/k)$, and $\hat{\dot{\theta}}_s(k/k)$ are computed from Eqs. (56)], into Eqs. (66) and (67).

2. Steady-State Approximation

Suppose that the difference equation (12), which describes the telescope dynamics, is stationary (i.e., the matrices Φ_t and Δ_t are

constant); this is equivalent to assuming that F_θ and D_θ of Eq. (11) are constant. This assumption is reasonable over a substantial time interval, since the rate of change of F_θ and D_θ is slow with respect to the system time constants. Additionally, it will be assumed that the summation in the performance criterion J of Eq. (41) is over an infinite time interval (i.e., $N = \infty$). This assumption is quite reasonable, since the interval of time during which the spacecraft is being tracked will be appreciably larger than the system time constants. With these two assumptions, computation of the optimal control u(k) is greatly simplified, as will be shown below. Formulation of the control problem in this manner will be referred to as the "steady-state approximation."

The Riccati equations (61) and (62) become

$$P_\varphi = A_\varphi + \Phi_\varphi^T P_\varphi \Phi_\varphi - \Phi_\varphi^T P_\varphi \Delta_\varphi \left[b_\varphi + \Delta_\varphi^T P_\varphi \Delta_\varphi \right]^{-1} \Delta_\varphi^T P_\varphi \Phi_\varphi \tag{68}$$

and

$$P_\theta = A_\theta + \Phi_\theta^T P_\theta \Phi_\theta - \Phi_\theta^T P_\theta \Delta_\theta \left[b_\theta + \Delta_\theta^T P_\theta \Delta_\theta \right]^{-1} \Delta_\theta^T P_\theta \Phi_\theta \quad . \tag{69}$$

The above are nonlinear algebraic equations in the steady-state matrices P_φ and P_θ, respectively. A possible way of solving these equations is to assume an initial solution, substitute it into the right-hand side, and evaluate a new solution; this iterative procedure is continued until successive solutions converge.

In addition, Eqs. (64) and (65) become

$$P_{3\varphi} = A_{3\varphi} + \Phi_d^T P_{3\varphi} \Phi_\varphi - \Phi_d^T P_{3\varphi} \Delta_\varphi \left[b_\varphi + \Delta_\varphi^T P_\varphi \Delta_\varphi \right]^{-1} \Delta_\varphi^T P_\varphi \Phi_\varphi \tag{70}$$

and

$$P_{3\theta} = A_{3\theta} + \Phi_h^T P_{3\theta} \Phi_\theta - \Phi_h^T P_{3\theta} \Delta_\theta \left[b_\theta + \Delta_\theta^T P_\theta \Delta_\theta \right]^{-1} \Delta_\theta^T P_\theta \Phi_\theta \quad . \tag{71}$$

Substituting P_φ and P_θ, the solutions to Eqs. (68) and (69), into the above linear algebraic equations enables one to solve for the steady-state matrices $P_{3\varphi}$ and $P_{3\theta}$ in a straightforward manner.

The control u(k) is obtained by substituting these steady-state matrices into Eqs. (66) and (67). Using the solutions to Eqs. (68) through (71) and performing the indicated matrix multiplications in Eqs. (66) and (67), it can be shown that the two components of the control have the form:

$$u_\varphi(k) = \gamma_{\varphi 1}[\hat{\varphi}_t(k/k) - \hat{\varphi}_s(k/k)] + \gamma_{\varphi 2}[\hat{\dot{\varphi}}_t(k/k) - \hat{\dot{\varphi}}_s(k/k)] + f_\varphi \hat{\dot{\varphi}}_s(k/k) \quad (72)$$

and

$$u_\theta(k) = \gamma_{\theta 1}[\hat{\theta}_t(k/k) - \hat{\theta}_s(k/k)] + \gamma_{\theta 2}[\hat{\dot{\theta}}_t(k/k) - \hat{\dot{\theta}}_s(k/k)] + f_\theta \hat{\dot{\theta}}_s(k/k), \quad (73)$$

The tracking system thus obtained develops controls that force the telescope and spacecraft angles and their angular rates to be equal (i.e., the first two terms in the control expressions are driven to zero). The third term provides the control input required to keep the telescope angular rate equal to that of the spacecraft, while maintaining zero steady-state tracking error. For a given set of system dynamics, $\gamma_{\varphi 1}$ and $\gamma_{\varphi 2}$ will be determined by the choice of b_φ; $\gamma_{\theta 1}$ and $\gamma_{\theta 2}$ will be determined by the choice of b_θ.

As a further refinement to the steady-state approximation, the time-varying nature of F_θ and D_θ can be taken into account as follows: F_θ and D_θ are periodically updated and Φ_θ and Δ_θ of Eq. (12) are recalculated. With these new matrices, P_θ [the solution to Eq. (69)] is recomputed. Finally, u_θ is obtained by using these updated matrices. Thus, a non-stationary problem is solved as a series of different stationary problems. It is not necessary to repeat this procedure at every discrete instant $k\Delta t$, since the rate of change of F_θ and D_θ is slow with respect to the system time constants.

IV AUTOTRACKER SYSTEM DESIGN

To permit a comparison of the performance levels achieved by the estimator-controller system configuration described in Sec. III and a tracking system of more conventional design, an autotrack control system was designed to operate with the same telescope structure and spacecraft dynamics as described in Sec. II-B. The design procedure followed in arriving at a satisfactory autotrack system design is described in this section.

For purposes of designing an autotrack system configuration for the earth-based terminal of the optical communication link, the block diagram for the declination channel can be drawn as shown in Fig. 5 (the hour-angle channel has identical form).

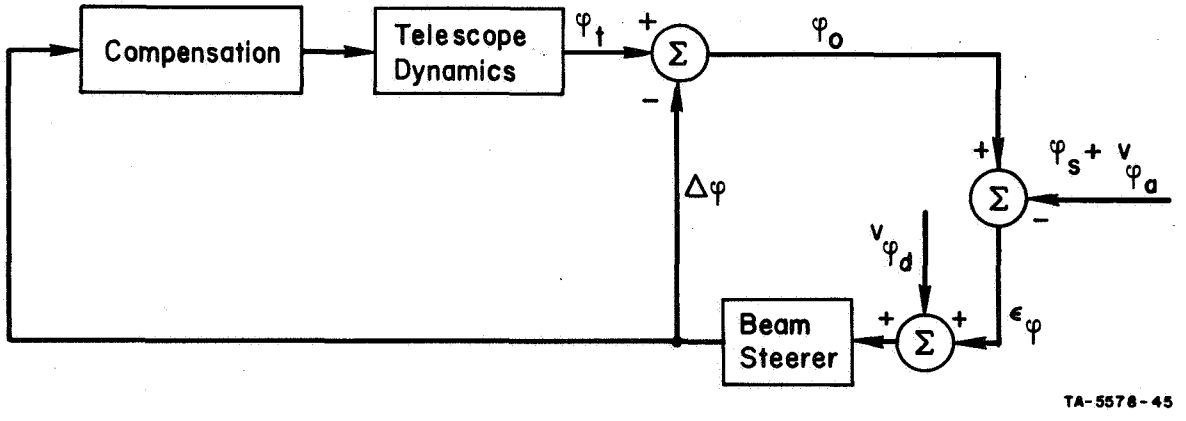

FIG. 5 AUTOTRACK SYSTEM (declination channel)

In Fig. 5, φ_t is the telescope mechanical axis, $\Delta\varphi$ is the offset angle provided by the beam steerer, φ_o is the optical axis, φ_s is the true angle to the spacecraft, v_{φ_a} is the atmospherically-induced disturbance, and v_{φ_d} is the measurement noise introduced by the optical detector. The figure can be simplified by noting that the bandwidth of the secondary loop containing the beam steerer is much larger than that of the remaining system; hence, its transmission

characteristics can be taken as unity. The primary loop of the telescope autotrack system then takes the form shown in Fig. 6, where v'_{φ_d} is the

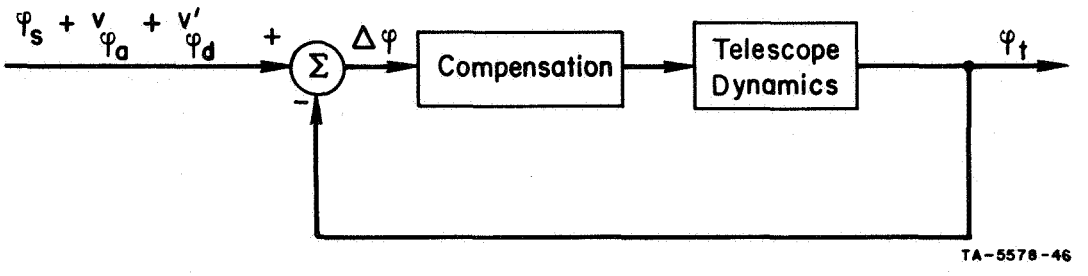

FIG. 6 PRIMARY TRACKING LOOP FOR AUTOTRACK SYSTEM
(declination channel)

measurement noise referred to the beam-steerer output. For the type of system being considered, the measurement noise is expected to be much smaller than the atmospherically-induced disturbances; hence, the input signal can be approximated by $\varphi_s + v_{\varphi_a}$. The ideal behavior of this system can be defined as the telescope mechanical axis following the true spacecraft direction and ignoring the atmospheric disturbances--i.e., $\varphi_t = \varphi_s$. The design problem thus reduces to the specification of a compensation network, which when used in conjunction with the dynamics of the telescope, will most closely approximate this ideal performance.

A suitable approximation for the telescope dynamics is obtained from the development given in Sec. II-B. From Eq. (11) of that development, the transfer function for the telescope dynamics is given by

$$G_\varphi(s) = \frac{\frac{1}{f_\varphi}}{s\left(\frac{J_\varphi}{f_\varphi}s + 1\right)} \tag{74}$$

for the declination axis, and

$$G_\theta(s) = \frac{\frac{1}{f_\theta}}{s\left(\frac{J_\theta}{f_\theta}s + 1\right)} \tag{75}$$

for the hour-angle axis (J_θ, which varies as a function of φ_t, is treated as a constant in order to express the above transfer function). Since these two are identical in form, only the declination axis will be treated in detail, and the results simply stated for the hour-angle axis.

As a first approach to the design of a compensation network, we consider the minimization of mean-square tracking error as formulated by Newton, Gould, and Kaiser.[10] Defining the power spectral density of φ_s as $\Phi_{ss}(s)$ and the power spectral density of the atmospheric disturbance as $\Phi_{vv}(s)$, the solution for the optimum compensation network takes the form

$$G_{c\varphi}(s) = \frac{1}{G_\varphi(s)} \left[\frac{\left\{ \dfrac{\Phi_{ss}(s)}{\Phi^-_{\sigma\sigma}(s)} \right\}_+}{\Phi^+_{\sigma\sigma}(s) + \left\{ \dfrac{\Phi_{ss}(s)}{\Phi^-_{\sigma\sigma}(s)} \right\}_+} \right] \tag{76}$$

where

$$\Phi_{\sigma\sigma}(s) = \Phi_{ss}(s) + \Phi_{vv}(s) \quad . \tag{77}$$

While this optimum compensation does yield maximal separation of the signal and noise power, and does not violate any physical realizability conditions, it has one serious shortcoming that removes it from consideration for use in a practical system. The first factor in Eq. (76), $1/G_\varphi(s)$, is the reciprocal of the telescope dynamics in the declination channel. The effect of this term, when the compensation is cascaded with the telescope, is to completely cancel the telescope dynamics. With the properties of the fixed portion of the system thus removed, the remaining terms of the compensation function then effect the optimum separation of the signal from the noise. Experience dictates, however, that any attempt at "pole cancellation" is doomed to failure since the performance of the resulting system is very sensitive to small parameter

changes and will most often become unstable if perfect cancellation is not achieved. Furthermore, if such an approach were attempted, the signal levels required throughout the system would certainly become so large as to violate the fundamental assumption of linearity, and thus invalidate the results.

The above exercise, however, does provide guidance in specifying a simple compensation network. The underlying principle is that if the power in the signal is separated in frequency from the power in the noise, then the frequency response of the system should be modified to respond to the signal but not to the noise. For a typical low satellite (200-mile altitude) the major portion of the signal power will be confined to frequencies below approximately 0.1 Hz; for higher satellites and deep-space probes it will be even lower in frequency.[11] On the other hand, measurements indicate that the atmospheric disturbances have a relatively uniform frequency distribution up to about 13 Hz, and decrease slowly for higher frequencies.[1] Thus, the most desirable approach is to set the system bandwidth near 0.1 Hz (0.68 rad/sec) so as to ensure adequate signal response and at the same time to eliminate as much of the noise as possible.

The above discussion assumes that load disturbances such as wind gusts need not be considered, since a high-precision telescope would be enclosed within a protective dome. For those cases where load disturbances might be encountered, the closed-loop system bandwidth is to a large extent determined by the requirement that the effect of the disturbance on the system output be minimal. Furthermore, the above argument does not consider the problem of target acquisition. For the very narrow field of view employed during tracking operations, the transient response implied by the closed-loop bandwidth chosen is much too sluggish to permit successful target acquisition by the tracking system. To accomplish acquisition it will most likely be necessary to increase the receiver field of view and the system bandwidth. These points are discussed in detail in Ref. 1, and need not be pursued further here.

It now remains to design a compensation network that will achieve the desired system performance as described above. A practical approach to this design problem (see, for example, Refs. 10 and 12) is to evaluate the system performance for compensation networks of increasing complexity until the desired behavior is attained.

Trying first a simple gain compensation $K_{\varphi 1}$ as shown in Fig. 7, the closed-loop transfer function is given by

$$\frac{1}{\frac{J_\varphi}{K_{\varphi 1}} s^2 + \frac{f_\varphi}{K_{\varphi 1}} s + 1} \quad . \tag{78}$$

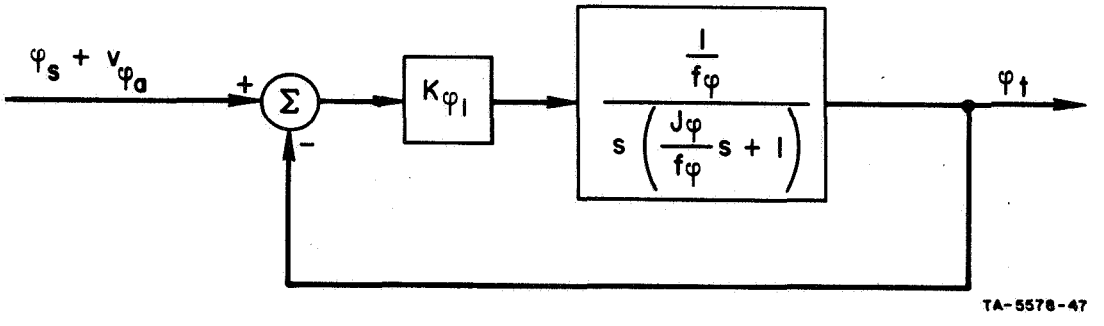

FIG. 7 AUTOTRACK SYSTEM WITH GAIN COMPENSATION
(declination channel)

The bandwidth is therefore

$$\omega_\varphi = \sqrt{\frac{K_{\varphi 1}}{J_\varphi}} \quad , \tag{79}$$

and for $\omega_\varphi = 0.628$ rad/sec,

$$K_{\varphi 1} = 7.5 \times 10^5 \quad . \tag{80}$$

The resulting system, however, displays two undesirable characteristics. First, the damping factor is only $\xi_{\varphi} = 0.0335$, which will yield highly oscillatory transient behavior and an amplification of approximately 15 for signals in the vicinity of the resonant frequency. Secondly, the system will display a steady-state tracking error to a ramp input as given by the expression

$$E_{ss_{\varphi}} = \frac{\Omega_i}{K_{v_{\varphi}}} \quad , \tag{81}$$

where Ω_i is the slope of the ramp input and $K_{v_{\varphi}}$ is the velocity constant. For the maximum expected rate of $\Omega_i = 7.28 \times 10^{-5}$ rad/sec and $K_{v_{\varphi}} = 9.4$, the steady-state tracking error in the declination channel is

$$E_{ss_{\varphi}} = 7.75 \times 10^{-6} \text{ rad} \quad . \tag{82}$$

While this tracking error is probably tolerable, the corresponding value for the hour-angle channel (where $K_{v_{\theta}} = 2.0$) is

$$E_{ss_{\theta}} = 3.64 \times 10^{-5} \text{ rad} \quad , \tag{83}$$

which is too large.

The first of these two difficulties can be alleviated by adding rate feedback as illustrated in Fig. 8. By proper adjustment of the rate feedback gain $K_{\varphi 2}$, the system damping factor can be adjusted to a more suitable value (such as $\xi_{\varphi} = 0.7$). Unfortunately, the addition of rate-feedback compensation has the effect of reducing the system velocity constant $K_{v_{\varphi}}$, thus aggravating the steady-state tracking error problem.

The most straightforward approach to curing the problem of steady-state tracking error is to add a series integration in the compensation network. Doing so yields the system configuration shown in Fig. 9.

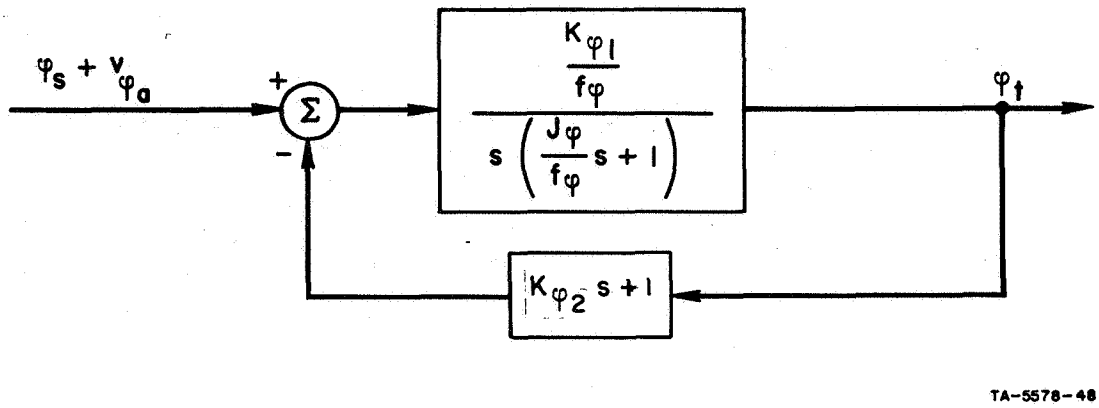

FIG. 8 AUTOTRACK SYSTEM WITH GAIN COMPENSATION AND RATE FEEDBACK (declination channel)

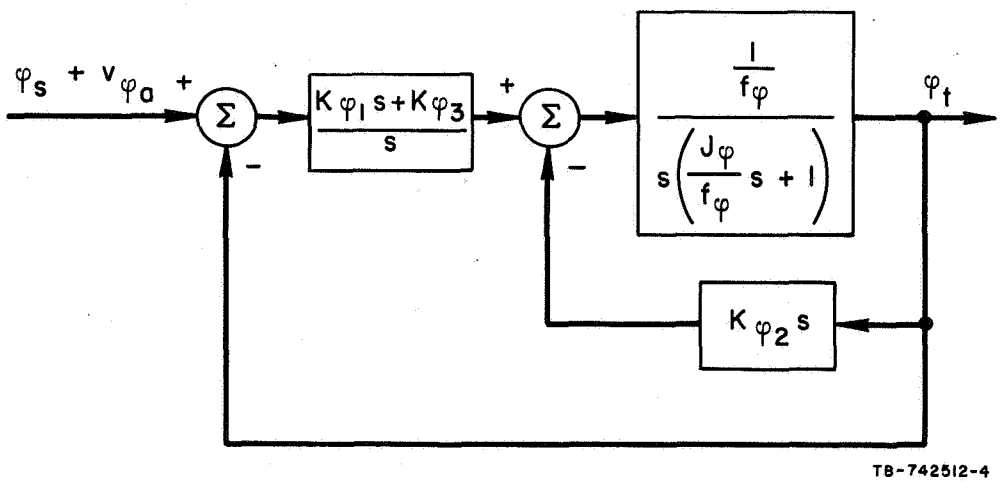

FIG. 9 AUTOTRACK SYSTEM WITH INTEGRAL FORWARD COMPENSATION AND INTERNAL RATE-LOOP COMPENSATION (declination channel)

This system design exhibits zero steady-state tracking error for a ramp input. The internal rate-loop compensation enables one to tailor the telescope dynamics. Having the three gains ($K_{\varphi 1}$, $K_{\varphi 2}$, and $K_{\varphi 3}$) permits complete flexibility in specifying the dynamic behavior of the system,

which is now third order. The closed-loop transfer function for the system configuration of Fig. 9 is given by

$$\frac{\frac{K_{\varphi 1}}{J_\varphi} s + \frac{K_{\varphi 3}}{J_\varphi}}{s^3 + \frac{f_\varphi + K_{\varphi 2}}{J_\varphi} s^2 + \frac{K_{\varphi 1}}{J_\varphi} s + \frac{K_{\varphi 3}}{J_\varphi}} \quad . \tag{84}$$

Written as the product of first and second order factors, this expression takes the form

$$\frac{(2a_\varphi \xi_\varphi \omega_\varphi + \omega_\varphi^2) s + a_\varphi \omega_\varphi^2}{(s + a_\varphi)(s^2 + 2\xi_\varphi \omega_\varphi s + \omega_\varphi^2)} \quad . \tag{85}$$

Choosing values of $a_\varphi = 1.0$, $\omega_\varphi = 0.5$, and $\xi_\varphi = 0.5$ will yield a net closed-loop system bandwidth in the order of 0.1 Hz as required, and a transient response that exhibits not more than 10-percent overshoot. The system gains that produce this performance are

$$\begin{aligned} K_{\varphi 1} &= 1.425 \times 10^6 \\ K_{\varphi 2} &= 2.765 \times 10^6 \\ K_{\varphi 3} &= 4.750 \times 10^5 \quad . \end{aligned} \tag{86}$$

Furthermore, since the feedback transmission is unity and there are now two integrations in the forward path, it is assured that this configuration will produce zero steady-state tracking error for a ramp input. Since this system configuration satisfies all of the stated design requirements for the autotrack system, it is the configuration used in the computer simulation of a tracking system of conventional design.

For the hour-angle axis, the only significant differences from the above analysis are the different values for J_θ and f_θ, and the variation of J_θ as a function of φ_t. Since φ_t changes very slowly, it is

reasonable to ignore higher-order and cross-coupling terms, and consider system performance as if J_θ were constant. To do this the system gains are chosen to produce the desired system characteristics for a nominal value of J_θ, and then the system characteristics are checked for the extreme values of J_θ. If no unacceptable variation occurs, then it is not necessary to vary the system gains as a function of φ_t to maintain acceptable performance. Taking J_θ to be 1.55×10^6, the gains that yield $a_\theta = 1.0$, $\omega_\theta = 0.5$, and $\xi_\theta = 0.5$ are

$$\begin{aligned} K_{\theta 1} &= 1.160 \times 10^6 \\ K_{\theta 2} &= 2.020 \times 10^6 \\ K_{\theta 3} &= 3.880 \times 10^5 \quad . \end{aligned} \tag{87}$$

Keeping the system gains at these values and varying J_θ over its range from a minimum of 0.6×10^6 to a maximum of 2.5×10^6 results in the following range of system properties. For the minimum value of J_θ, the parameter values of the closed-loop transfer function are

$$a_\theta = 3.36, \ \omega_\theta = 0.438, \text{ and } \xi_\theta = 0.594. \tag{88}$$

The small decrease in resonant frequency indicated will be more than compensated by the increase in a_θ; hence, the system behavior should be essentially unchanged from the nominal for these conditions. For the maximum value of J_θ, the parameter values of the closed-loop transfer function are

$$a_\theta = 0.587, \ \omega_\theta = 0.518, \text{ and } \xi_\theta = 0.332. \tag{89}$$

The significant variations in this case are the reductions in a_θ and ξ_θ. The reduced a_θ would be expected to reduce the system bandwidth below the design value of 0.5 rad/sec; however, the resonant amplification of approximately 2.0, associated with a damping factor of 0.332, will compensate for this bandwidth reduction and lead to a net system bandwidth

in the vicinity of 0.5 rad/sec. Conversely, one would expect the low damping to lead to large transient overshoots. However, the single pole at $a_\theta = 0.587$ will partially compensate for the overshoot, reducing it from a maximum value of 30 percent to a maximum value of approximately 15 percent. Hence, even though the parameter values appear to change appreciably, the net system performance will remain acceptably close to the nominal design values.

Since it has been shown that the system performance remains satisfactory over the entire range of values that can be assumed by J_θ, and that the rate of variation is small enough to permit ignoring cross-coupling terms, it is therefore reasonable to implement the system with just one set of fixed gains as given in Eqs. (87).

It should be noted that the telescope's angular position and rate, which are fed back through the compensation network, will actually be corrupted by measurement noise. This effect has been included in the computer simulation of the autotrack system.

V PERFORMANCE TESTING OF TRACKING SYSTEMS

The tracking system configurations proposed and analyzed in Secs. III and IV have been simulated by means of a digital computer. This simulation permits the evaluation of performance levels achieved by each of the system designs as well as direct comparisons of their performance capabilities under similar operating conditions. The program is set up to simulate the operation of the earth-terminal tracking system as if it were tracking an optical signal originating at a spacecraft in the vicinity of Mars. The program has been written in Fortran IV (Version 13) and runs on the IBM-DCS 7040-7094 at the NASA Ames Research Center.[13] The approximate execution time per iteration is 0.36 seconds for the estimator-controller configuration, and 0.08 seconds for the autotracker system.

For the simulation tests that were conducted, two forms of system performance are computed and plotted versus time. The first performance measure plotted is the angular estimation error--the angular difference between the direction of signal arrival as obtained at the data readout points and the true direction of signal arrival--in terms of the declination and hour angles. For the estimator-controller configuration, the data readouts are the estimates of the spacecraft angles that are obtained from the estimate of the spacecraft state [see Fig. 1 and Eqs. (56)]; whereas for the autotrack configuration, the data readout points are taken to be the digital encoders that measure the angular positions of the telescope axes (see Figs. 5 and 6). The second performance measure is the angular tracking error--the angular difference between the telescope axis and the direction of signal arrival--in both the declination and hour-angle axes. These plots indicate the performance of the tracking system in maintaining proper pointing of the telescope axis. It is important to point out the distinction between these two performance measures, since the second bears on the system's ability to maintain continuous communication contact while the first is pertinent to the

quality of the data that the system can produce for such purposes as spacecraft trajectory determination.

The a priori state estimate $\hat{x}(0/0)$ and its error covariance $P(0/0)$ are used to initialize the recursive equations for the estimator. Two different sets of initial state estimates $\hat{x}(0/0)$ of the initial conditions $x(0)$ for the actual test data, together with the resulting spacecraft angles [$\hat{\varphi}_s(0/0)$, $\hat{\theta}_s(0/0)$ and $\varphi_s(0)$, $\theta_s(0)$ respectively], are specified in Table I. Cases 1 and 2 are representative of the numerous examples that were simulated for the estimator-controller configuration. The operation of the autotracker was also simulated, using the actual test data given in Table I. The best values for $P(0/0)$, the covariance of the error in the initial state estimate defined in Eq. (28), and for $Q(k)$, the covariance of the random disturbance defined in Eq. (27), were determined experimentally to be

$$P(0/0) = \begin{bmatrix} 5 \times 10^{19} & & & & & & & & \\ & 5 \times 10^{19} & & & & & & & \\ & & 0 & & & & & & \\ & & & 10^{2} & & & & & \\ & & & & 10^{2} & & & & \\ & & & & & 0 & & & \\ & & & & & & 10^{-9} & & \\ & & & & & & & 10^{-6} & \\ & & & & & & & & 10^{-9} \\ & & & & & & & & & 10^{-6} \end{bmatrix} \tag{90}$$

$$\frac{Q(k)}{(\Delta t)^2} = \begin{bmatrix} 0 & & & & & & & & \\ & 0 & & & & & & & \\ & & 0 & & & & & & \\ & & & 2 \times 10^{3} & & & & & \\ & & & & 2 \times 10^{3} & & & & \\ & & & & & 0 & & & \\ & & & & & & 0 & & \\ & & & & & & & 10^{-11} & \\ & & & & & & & & 0 \\ & & & & & & & & & 10^{-12} \end{bmatrix} . \tag{91}$$

Table I

INITIAL CONDITIONS

	Actual $x(0)$	Case 1 $\hat{x}(0/0)$	Case 2 $\hat{x}(0/0)$
x_{1_s} (m)	1.2000×10^{11}	1.1998×10^{11}	1.2002×10^{11}
x_{2_s} (m)	1.6000×10^{11}	1.6002×10^{11}	1.5998×10^{11}
x_{3_s} (m)	0	0	0
$\dot{x}_{1_s}$ (m/sec)	-8.000×10^{3}	-8.002×10^{3}	-8.002×10^{3}
$\dot{x}_{2_s}$ (m/sec)	7.000×10^{3}	7.003×10^{3}	7.003×10^{3}
$\dot{x}_{3_s}$ (m/sec)	0	0	0
φ_t (rad)	-0.0711750	-0.0711700	-0.0711700
$\dot{\varphi}_t$ (rad/sec)	0	0	0
θ_t (rad)	0.1647270	0.1647300	0.1647300
$\dot{\theta}_t$ (rad/sec)	0	10^{-4}	10^{-4}
φ_s (rad)	-0.0711754	-0.0712144	-0.0711364
θ_s (rad)	0.1647272	0.1648185	0.1646358

The units on these variances correspond to those given in Table I. For an Earth-Mars mission it is reasonable to assume that the trajectory of the spacecraft lies in the plane of the ecliptic. Hence, $x_{3_s} = \dot{x}_{3_s} = 0$, and the corresponding variances in Eqs. (90) and (91) can be set equal to zero.

For the estimator-controller, R(k), the covariance of the measurement noise, is given in Eqs. (25) and (26). For the autotracker, the noise introduced by image excursion and the noise on the measurements of the telescope's angular position are as given in Eqs. (26). The measurement noises for the telescope's angular rate are taken to have a variance of $9 \times 10^{-12} (\text{rad/sec})^2$.

The cost associated with control, as characterized by b_φ and b_θ [see Eq. (41)], determines the performance of the controller. The best values for these quantities were determined experimentally to be

$$b_\varphi = 10^{-10}$$
$$b_\theta = 10^{-11} \quad . \tag{92}$$

The ultimate limitation on the performance of the optical communication and tracking system is dictated by the magnitude of the atmospheric-induced image excursion, as characterized by σ_{φ_a} and σ_{θ_a}. Hence, to determine the sensitivity of system performance to image excursion, σ_{φ_a} and σ_{θ_a} were varied about their nominal values of 15×10^{-6} rad (where 1.0 arc sec = 4.85×10^{-6} rad). The results of these computer runs are presented in Figs. 10 through 15 for the estimator-controller (Cases 1 and 2) and in Figs. 16 through 18 for the autotracker, with a nominal interation interval $\Delta t = 0.25$ sec. These figures indicate that under similar operating conditions the performance (estimation and tracking errors) of the estimator-controller is appreciably better than that of the autotracker.* Furthermore, the performance of the

*It should be noted that the results for the estimator-controller are plotted on a scale of $\pm 10 \times 10^{-6}$ rad, while the results for the autotracker are plotted on a scale of $\pm 50 \times 10^{-6}$ rad.

estimator-controller configuration is less sensitive to increases in atmospheric disturbances than is the autotracker system. In addition, the results in Figs. 10 through 15 for Cases 1 and 2 demonstrate that the convergence properties of the estimator are essentially independent of the a priori state estimate [for reasonable choices of $\hat{x}(0/0)$].

Another set of tests were conducted to determine the sensitivity of estimator performance to the iteration interval Δt. Only the performance of the estimator was considered in these computer runs, because it has been found that iteration intervals much in excess of the nominal 0.25 sec introduce spurious dynamic effects into the simulation of the controller and telescope behavior. The estimator was operated at interation intervals of $\Delta t = 1.0$ second and $\Delta t = 2.0$ seconds for Cases 1 and 2, with the nominal noise conditions described above. The results of these tests, shown in Figs. 19 through 22, illustrate that there is only a slight degradation in performance for increased Δt.

For the purpose of minimizing the system computer requirements in an actual implementation, multirate operation should be considered, where the iteration interval for the controller is set small so as to ensure smooth telescope behavior, while the iteration interval of the estimator is made large to reduce the total computation time required. This multirate operation can afford a considerable saving in total computation time (and thus in required machine speed) since the estimator presently accounts for approximately 95 percent of the computation time per iteration.

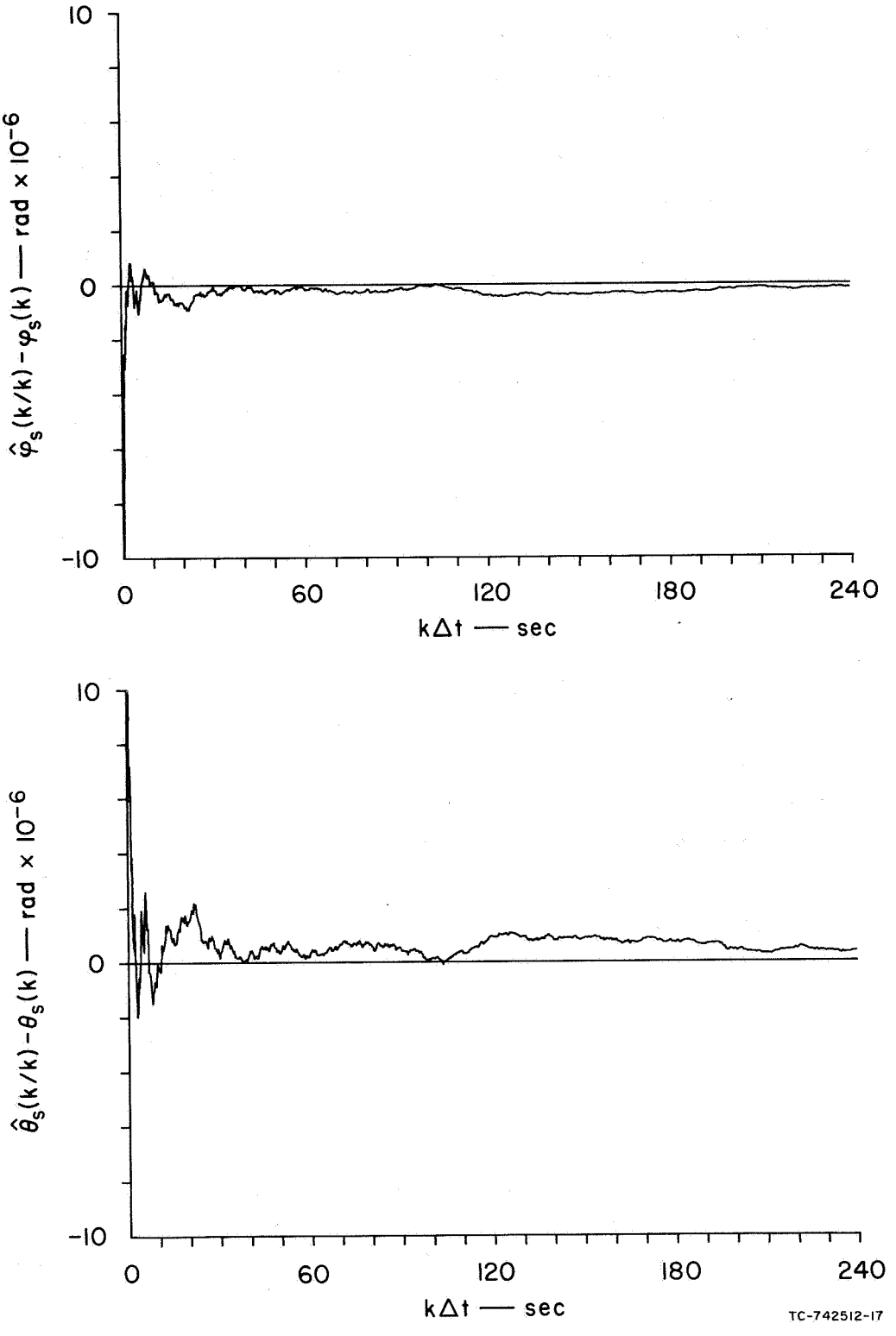

(a) ESTIMATION ERRORS

FIG. 10 ESTIMATOR-CONTROLLER (Case 1), $\sigma_{\varphi_a} = \sigma_{\theta_a} = 15 \times 10^{-6}$ rad, $\Delta t = 0.25$ sec

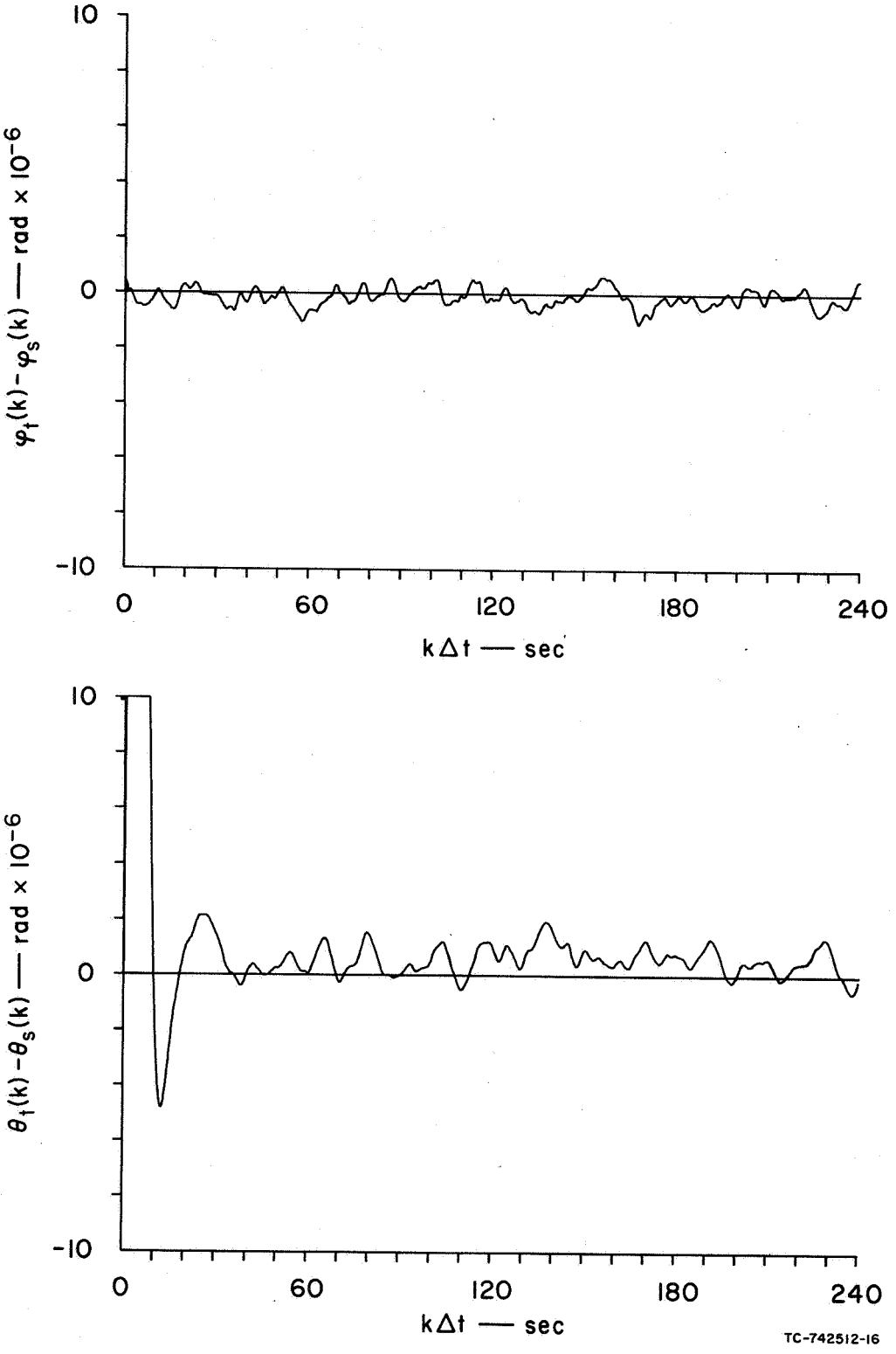

(b) TRACKING ERRORS

FIG. 10 Concluded

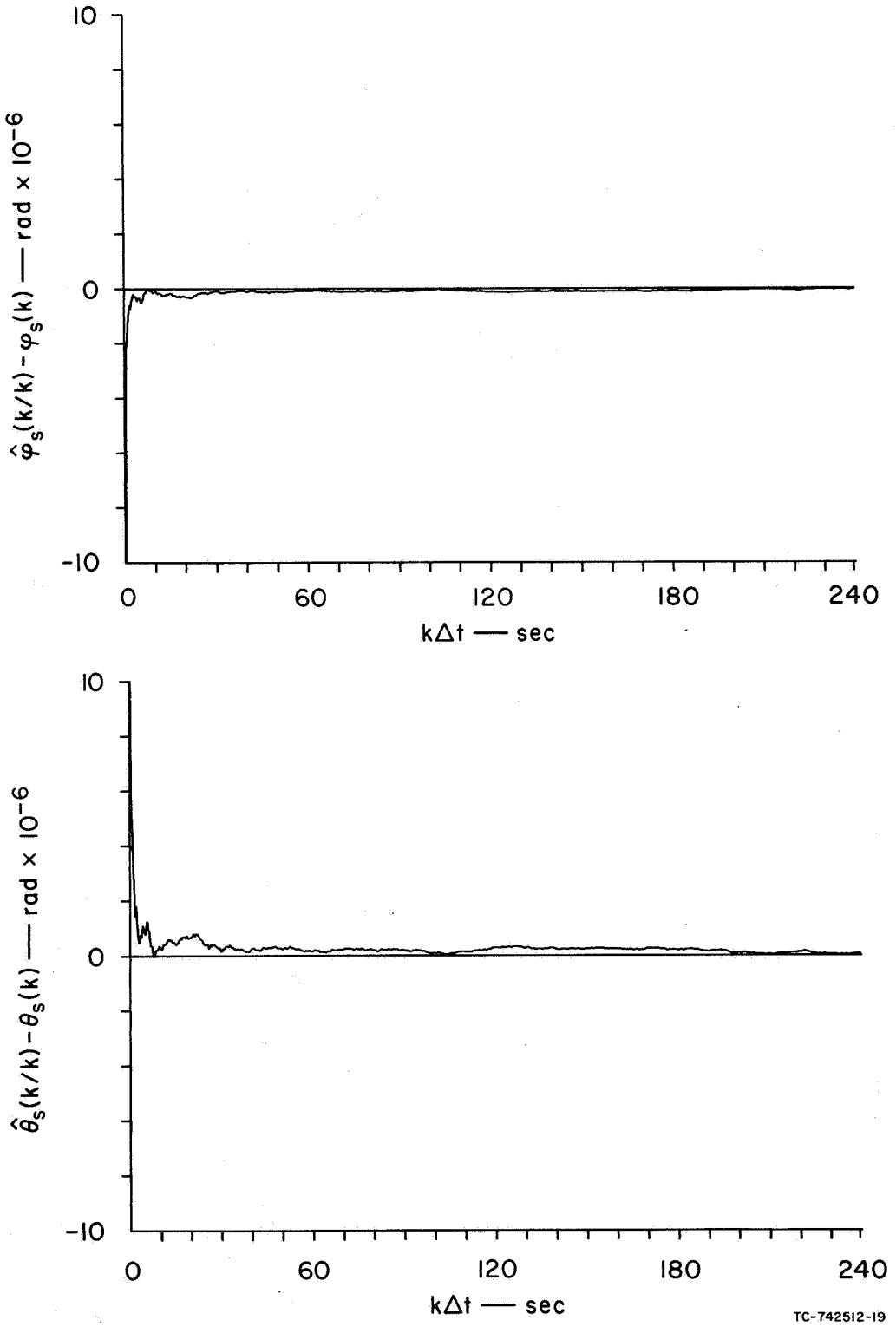

(a) ESTIMATION ERRORS

FIG. 11 ESTIMATOR–CONTROLLER (Case 1), $\sigma_{\varphi_a} = \sigma_{\theta_a} = 3.75 \times 10^{-6}$ rad, $\Delta t = 0.25$ sec

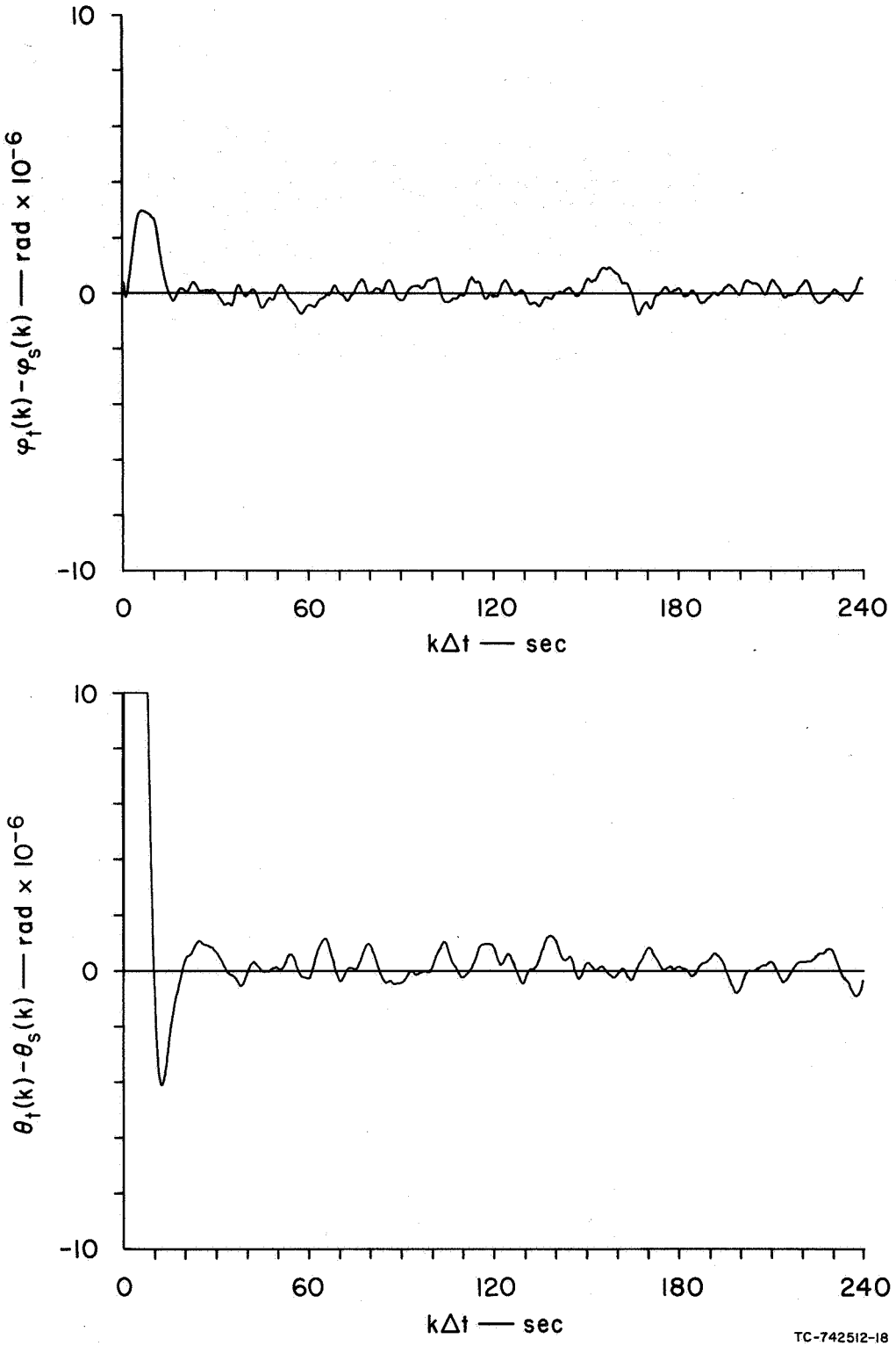

(b) TRACKING ERRORS

FIG. 11 Concluded

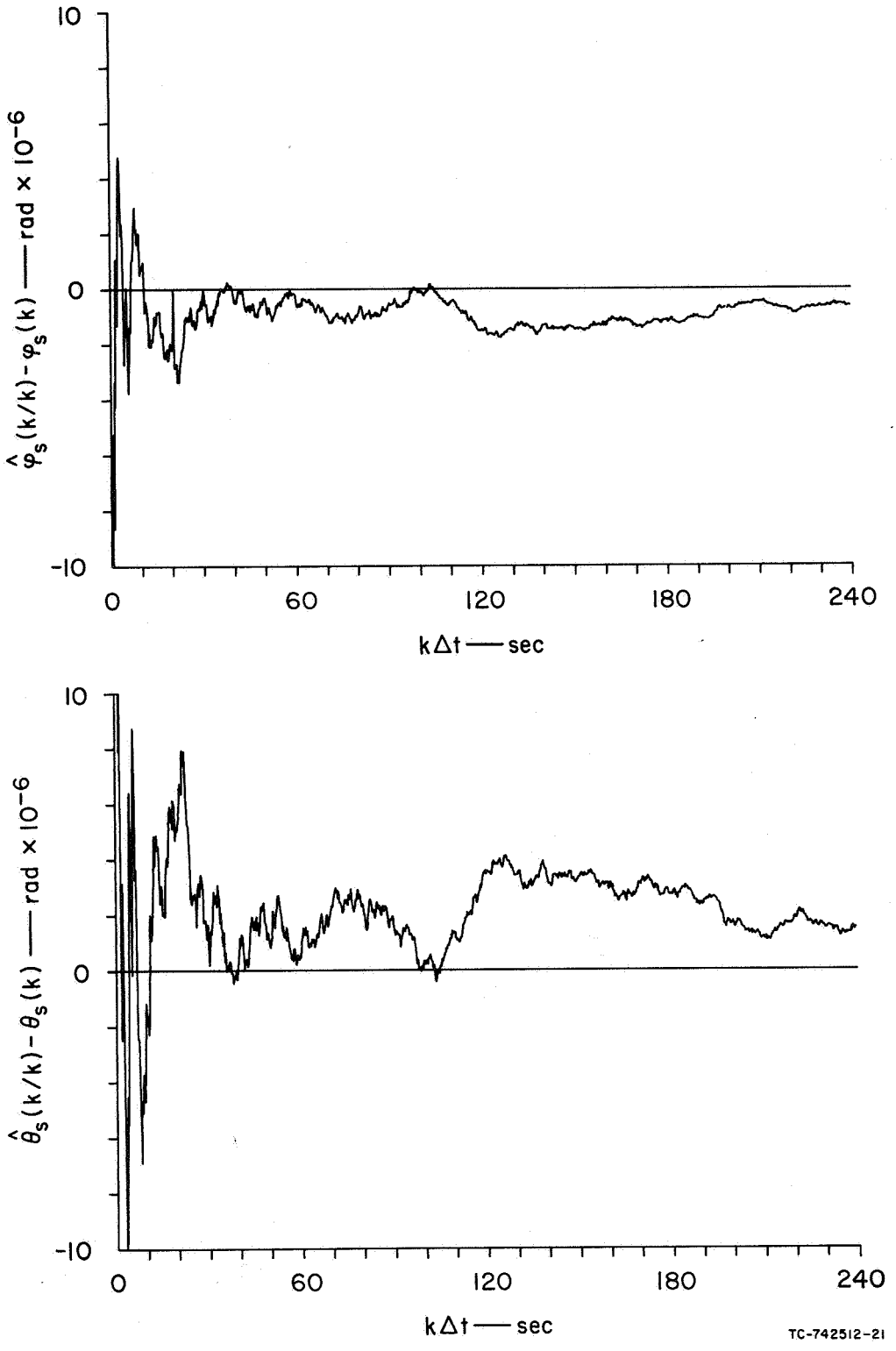

(a) ESTIMATION ERRORS

FIG. 12 ESTIMATOR-CONTROLLER (Case 1), $\sigma_{\varphi_a} = \sigma_{\theta_a} = 60 \times 10^{-6}$ rad, $\Delta t = 0.25$ sec

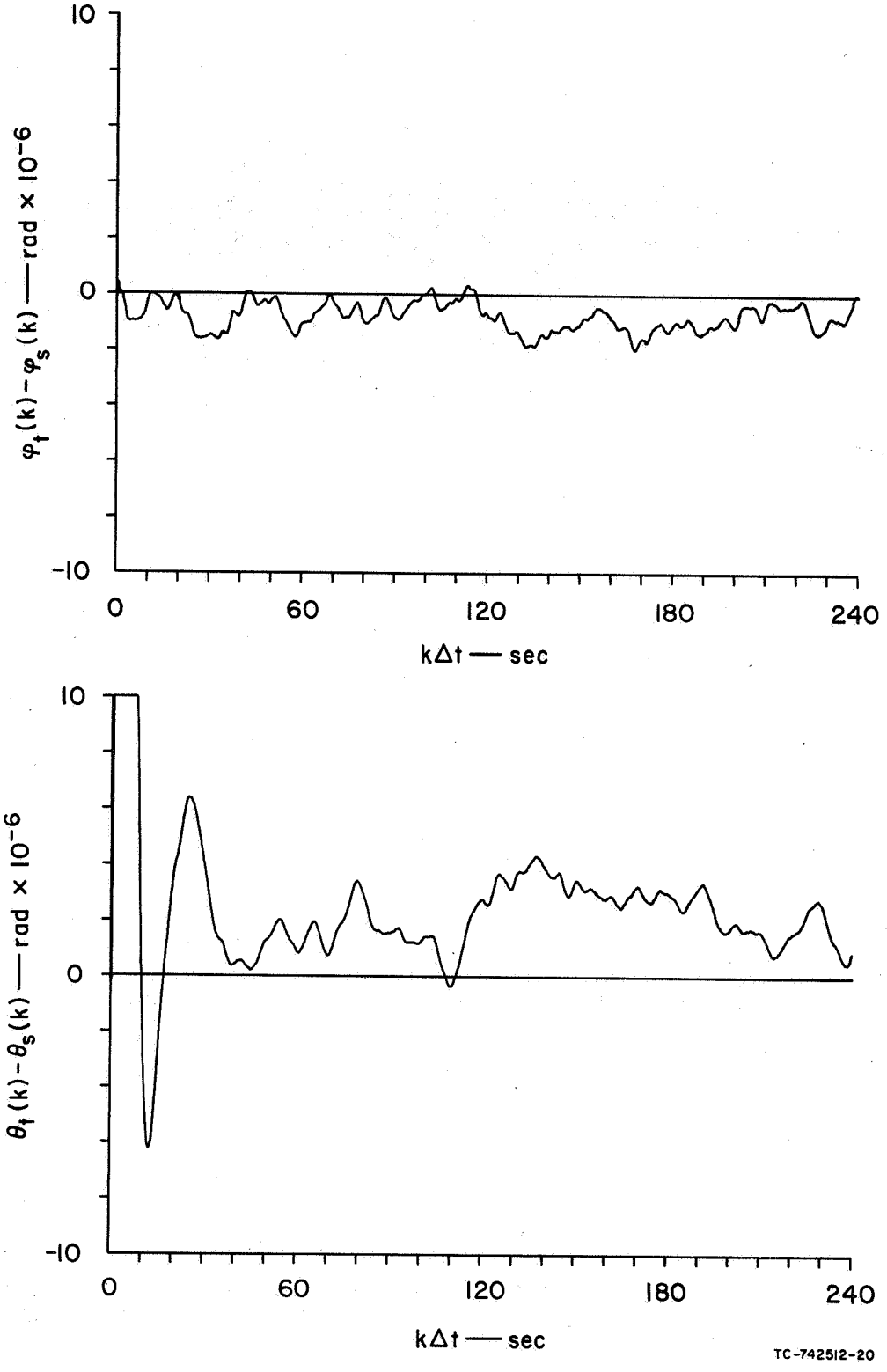

(b) TRACKING ERRORS

FIG. 12 Concluded

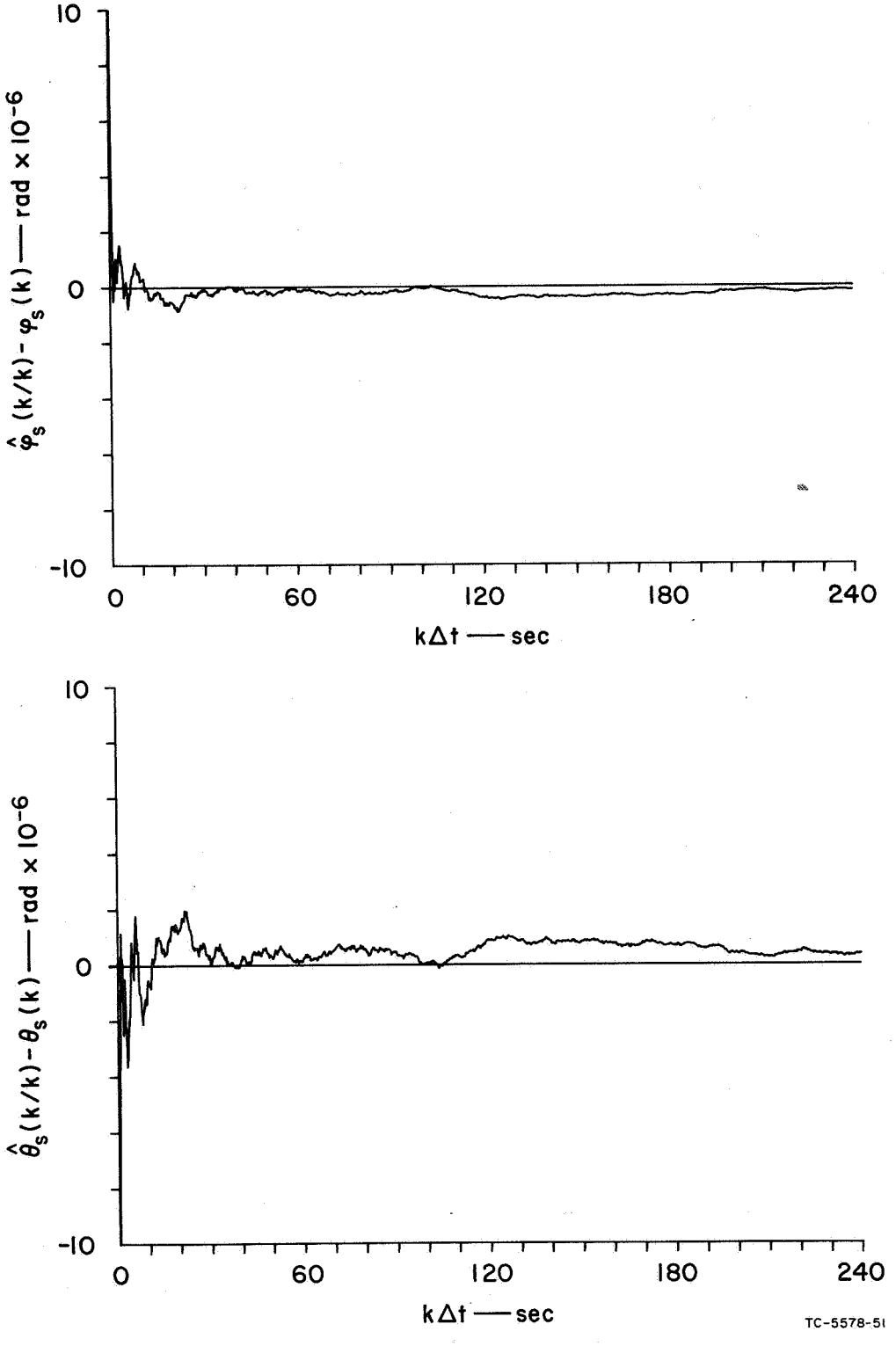

(a) ESTIMATION ERRORS

FIG. 13 ESTIMATOR–CONTROLLER (Case 2), $\sigma_{\varphi_a} = \sigma_{\theta_a} = 15 \times 10^{-6}$ rad, $\Delta t = 0.25$ sec

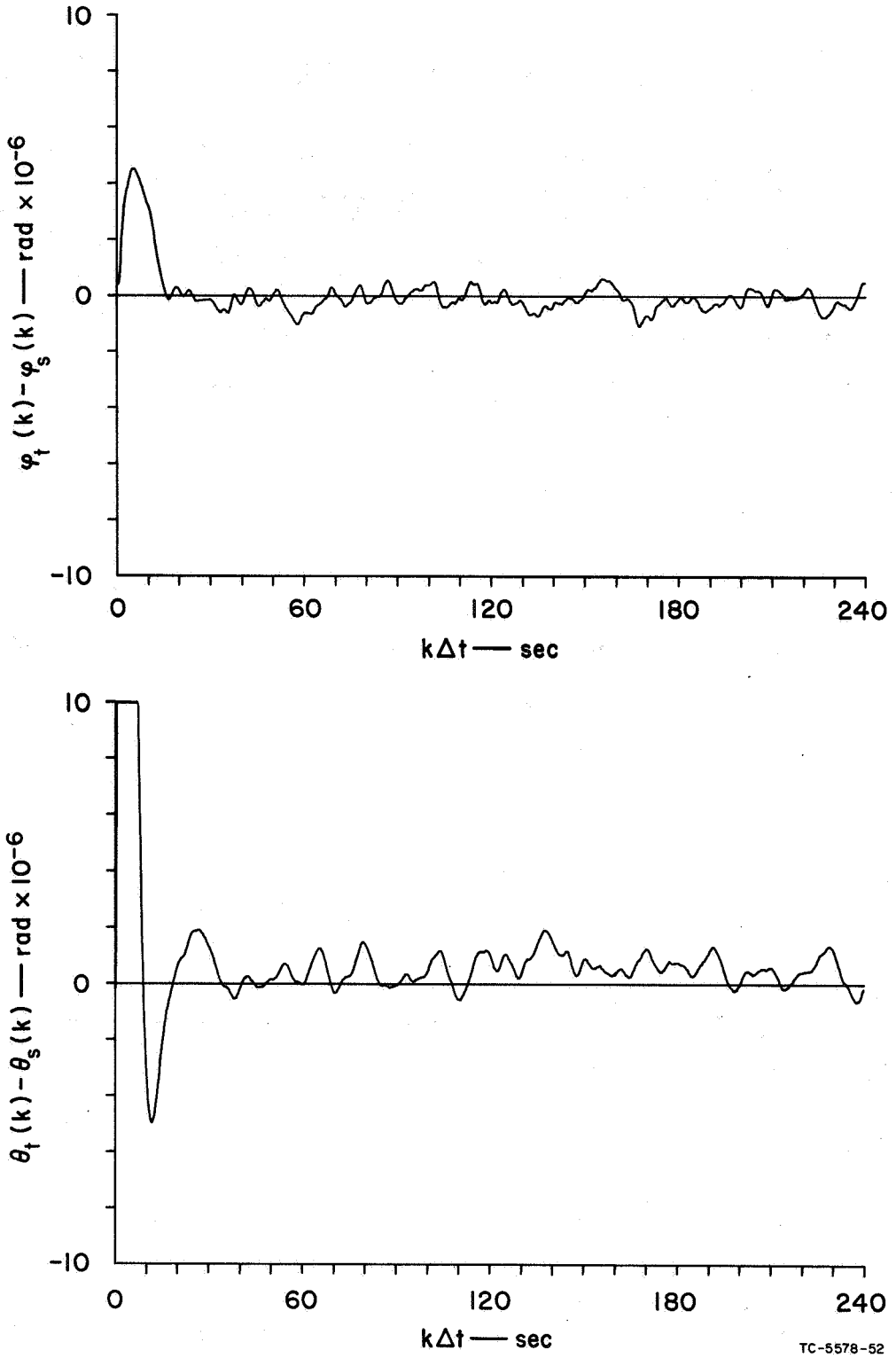

(b) TRACKING ERRORS

FIG. 13 Concluded

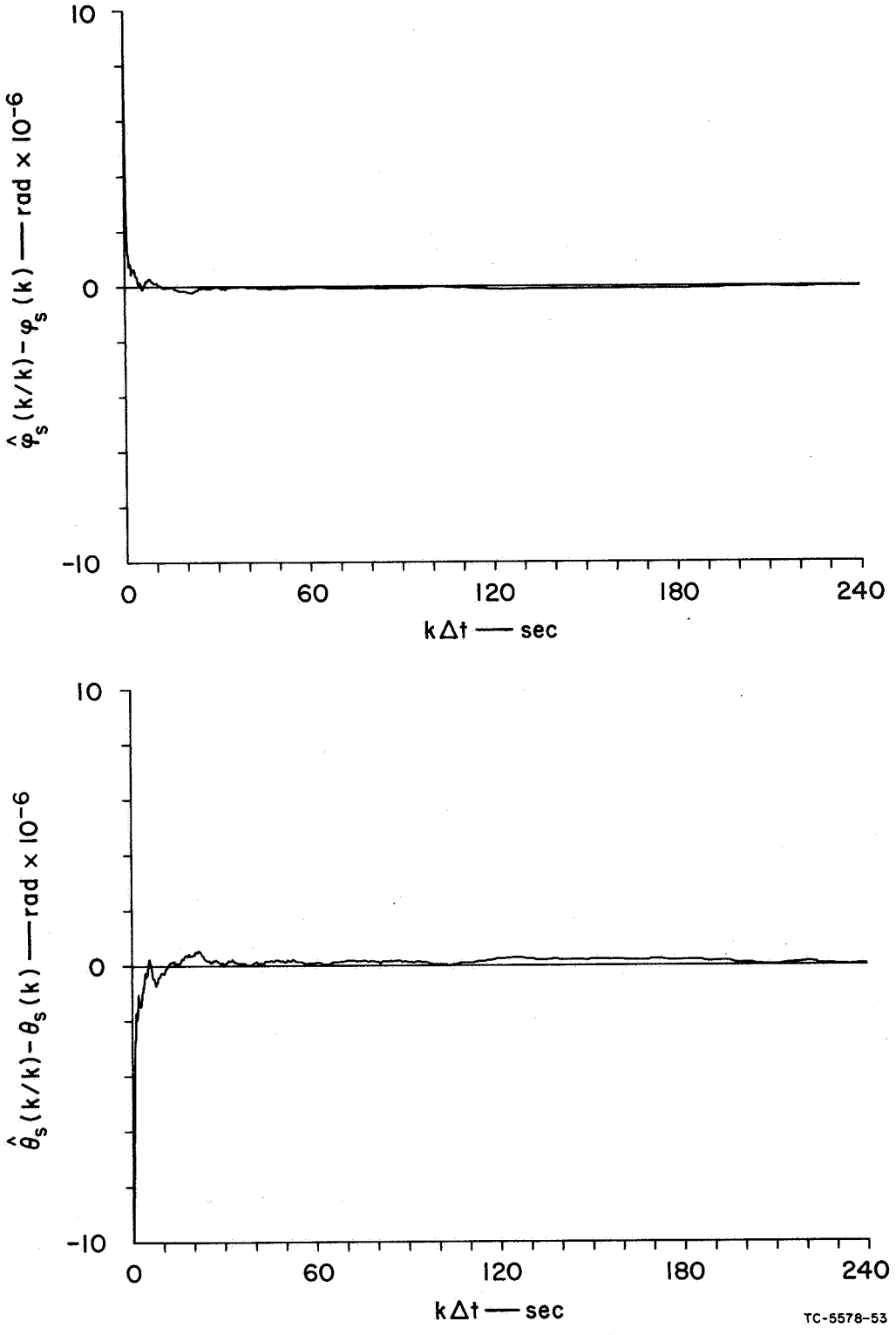

(a) ESTIMATION ERRORS

FIG. 14 ESTIMATOR–CONTROLLER (Case 2), $\sigma_{\varphi_a} = \sigma_{\theta_a} = 3.75 \times 10^{-6}$ rad, $\Delta t = 0.25$ sec

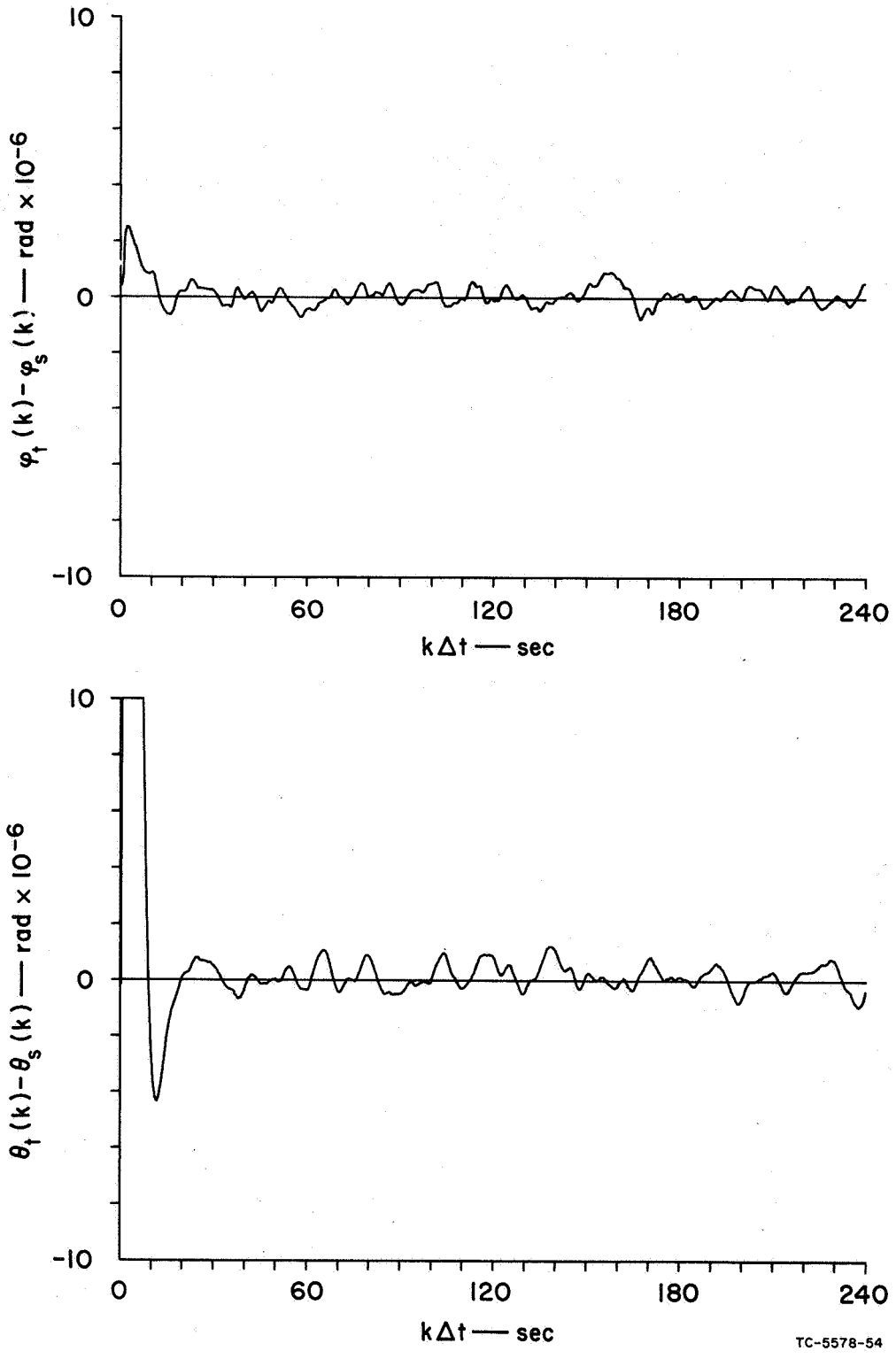

(b) TRACKING ERRORS

FIG. 14 Concluded

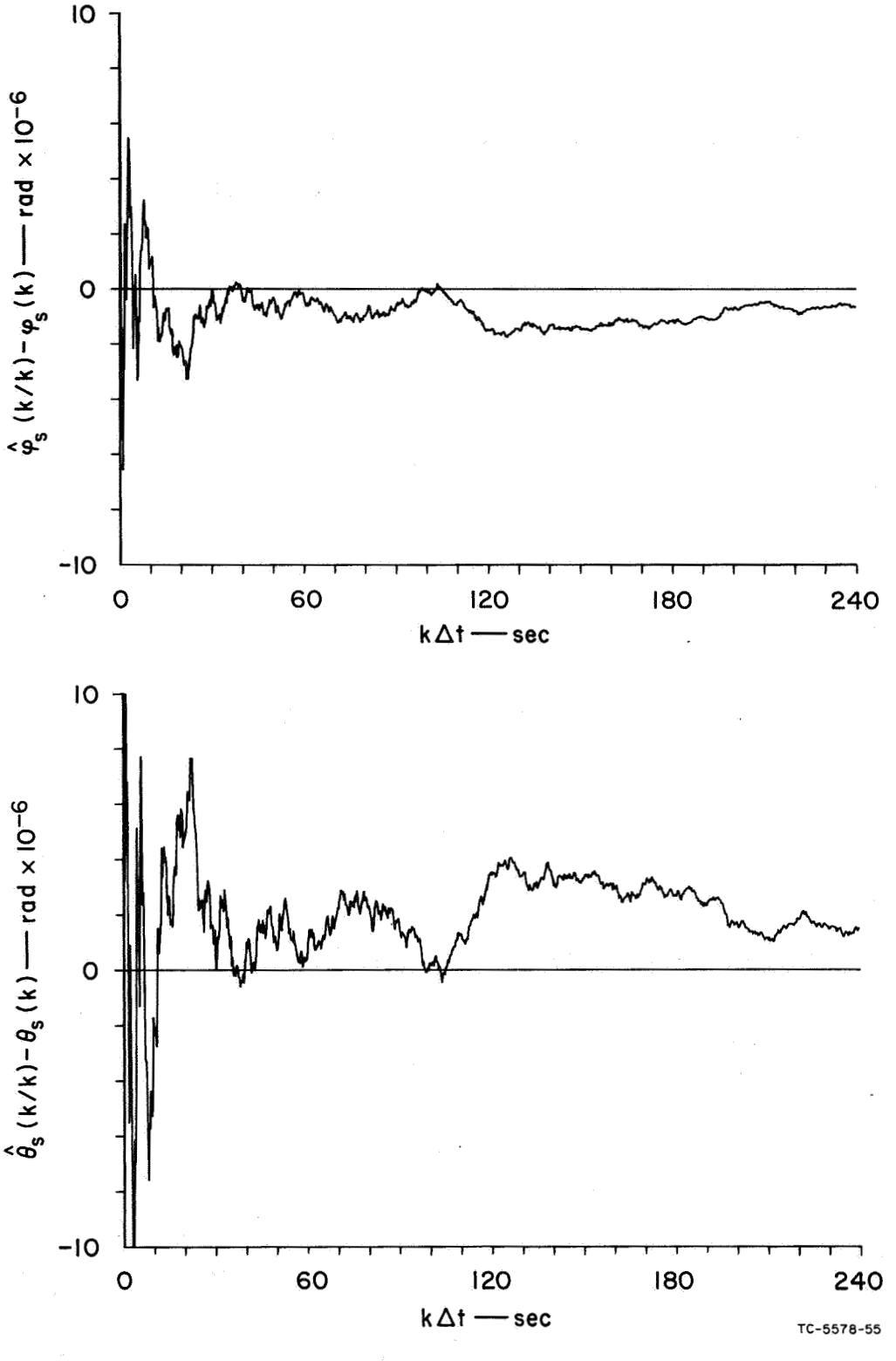

(a) ESTIMATION ERRORS

FIG. 15 ESTIMATOR–CONTROLLER (Case 2), $\sigma_{\varphi_a} = \sigma_{\theta_a} = 60 \times 10^{-6}$ rad, $\Delta t = 0.25$ sec

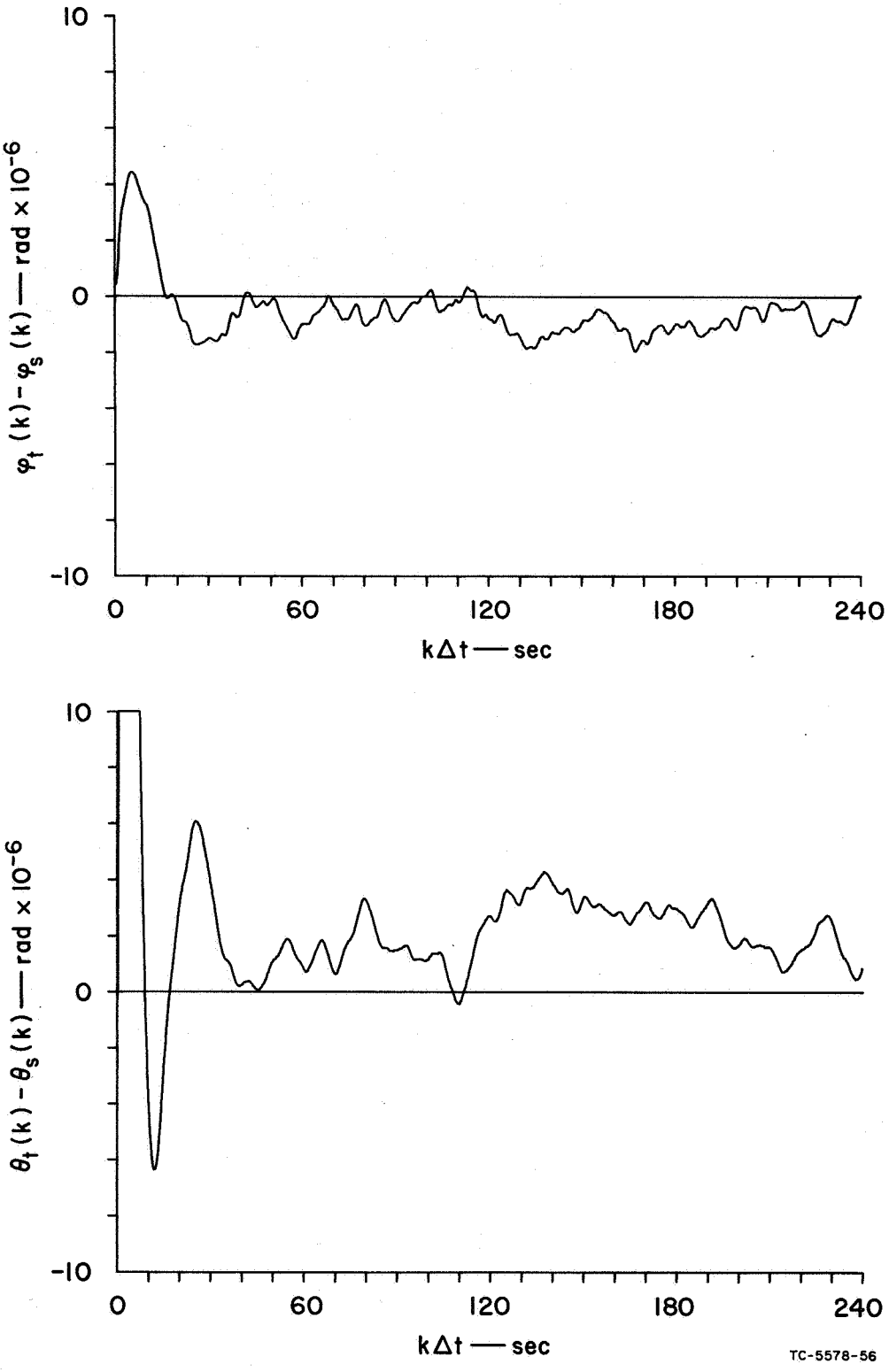

(b) TRACKING ERRORS

FIG. 15 Concluded

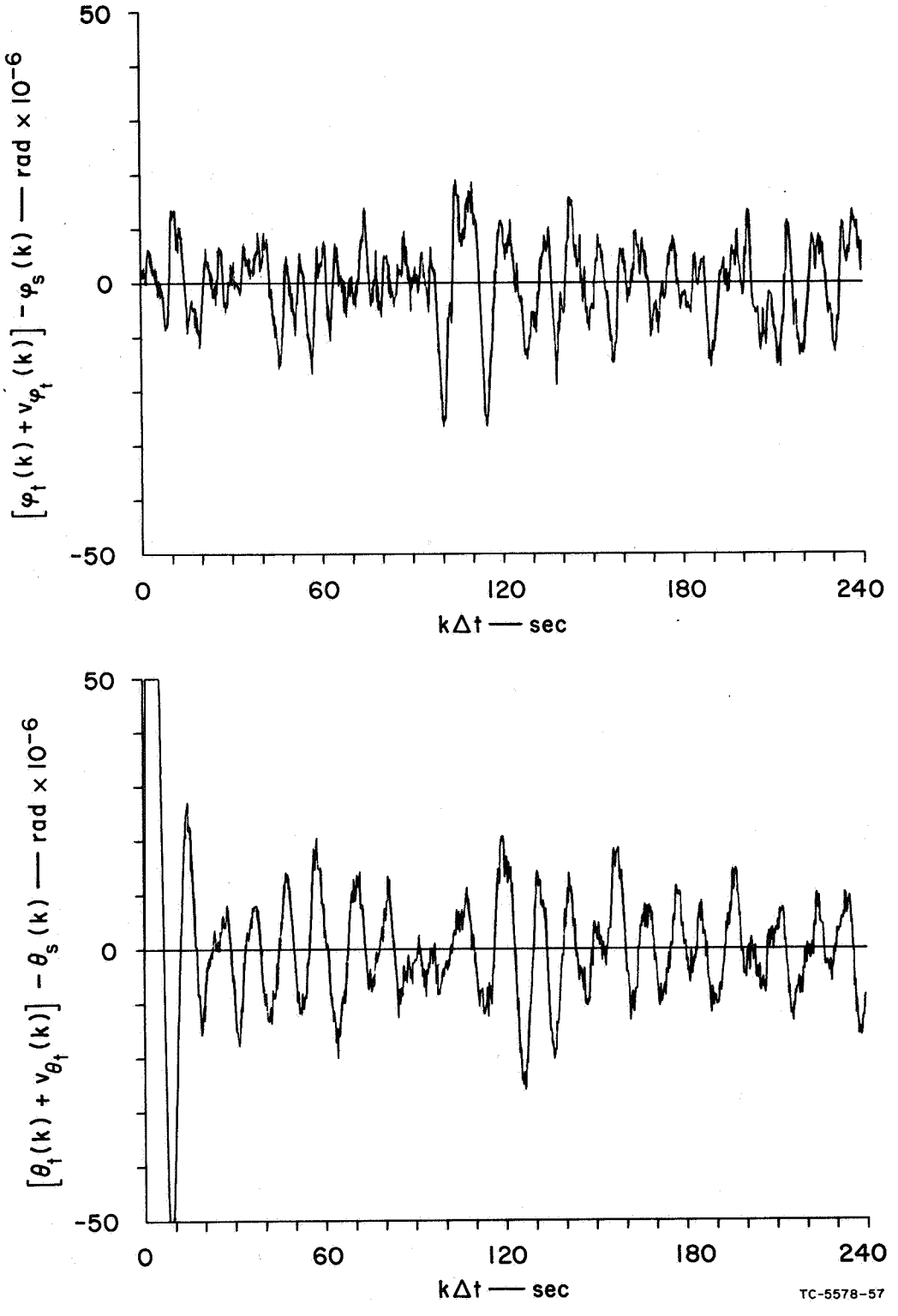

(a) ESTIMATION ERRORS

FIG. 16 AUTOTRACKER, $\sigma_{\varphi_a} = \sigma_{\theta_a} = 15 \times 10^{-6}$ rad, $\Delta t = 0.25$ sec

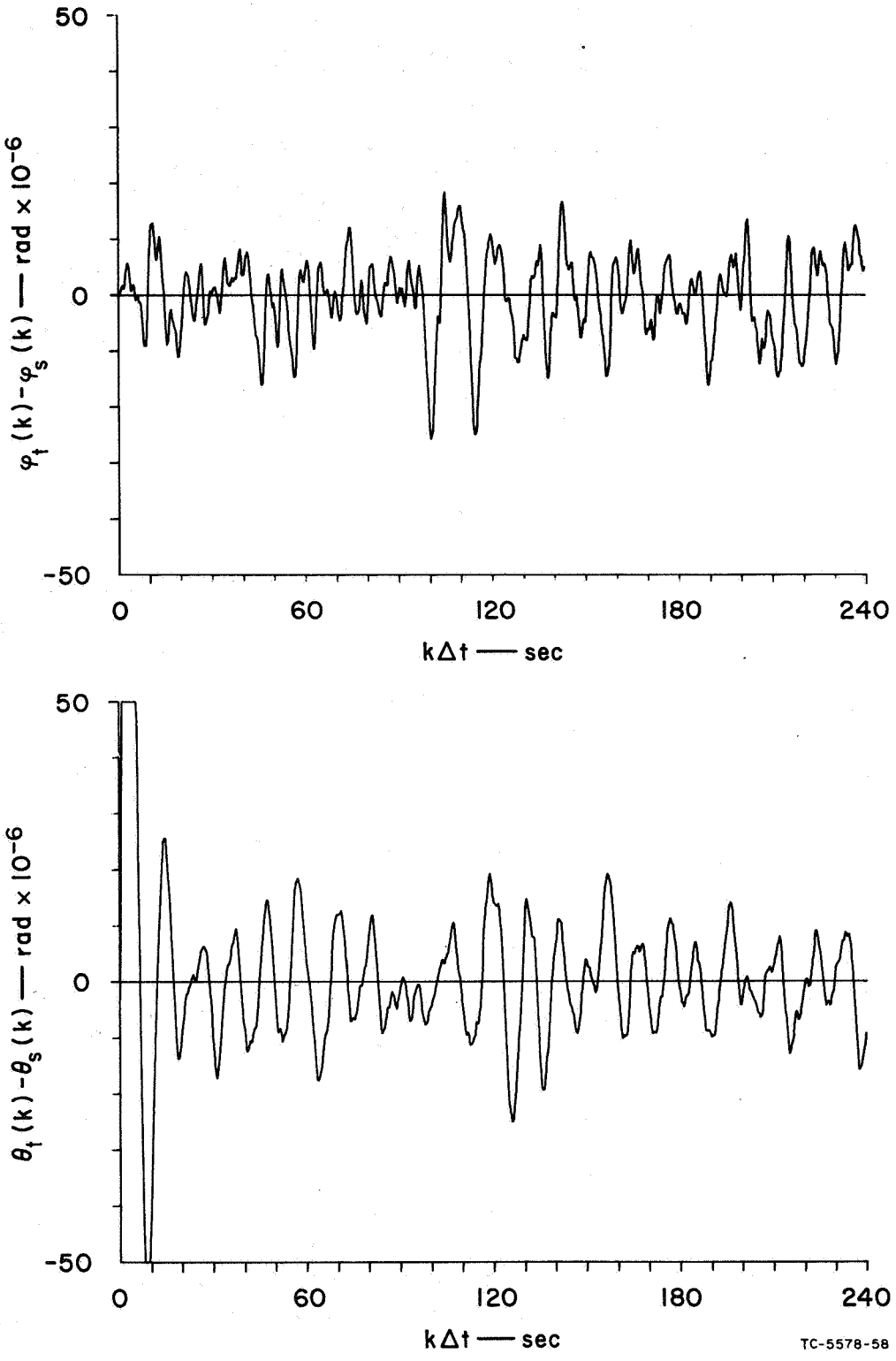

(b) TRACKING ERRORS

FIG. 16 Concluded

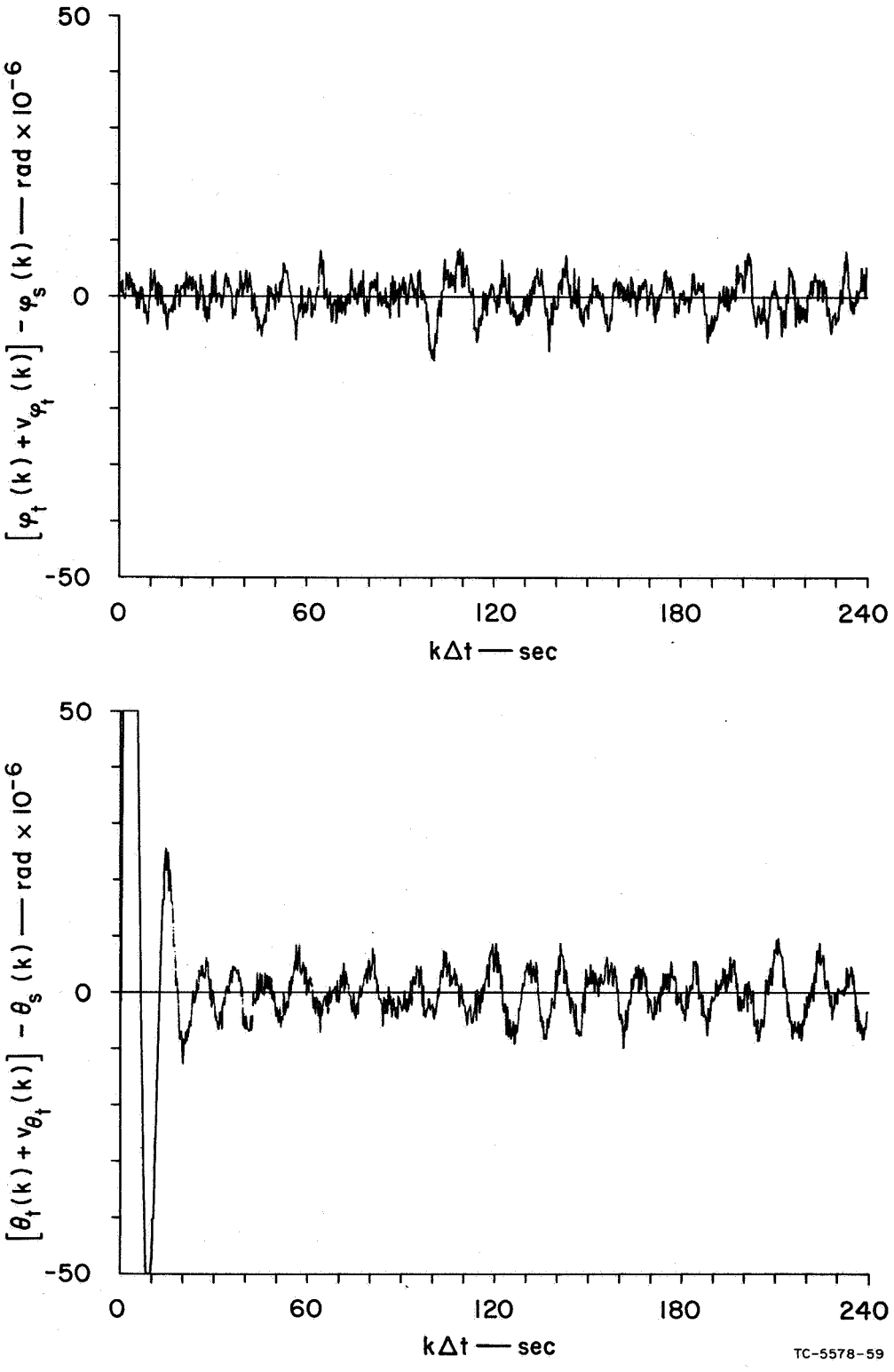

(a) ESTIMATION ERRORS

FIG. 17 AUTOTRACKER, $\sigma_{\varphi_a} = \sigma_{\theta_a} = 3.75 \times 10^{-6}$ rad, $\Delta t = 0.25$ sec

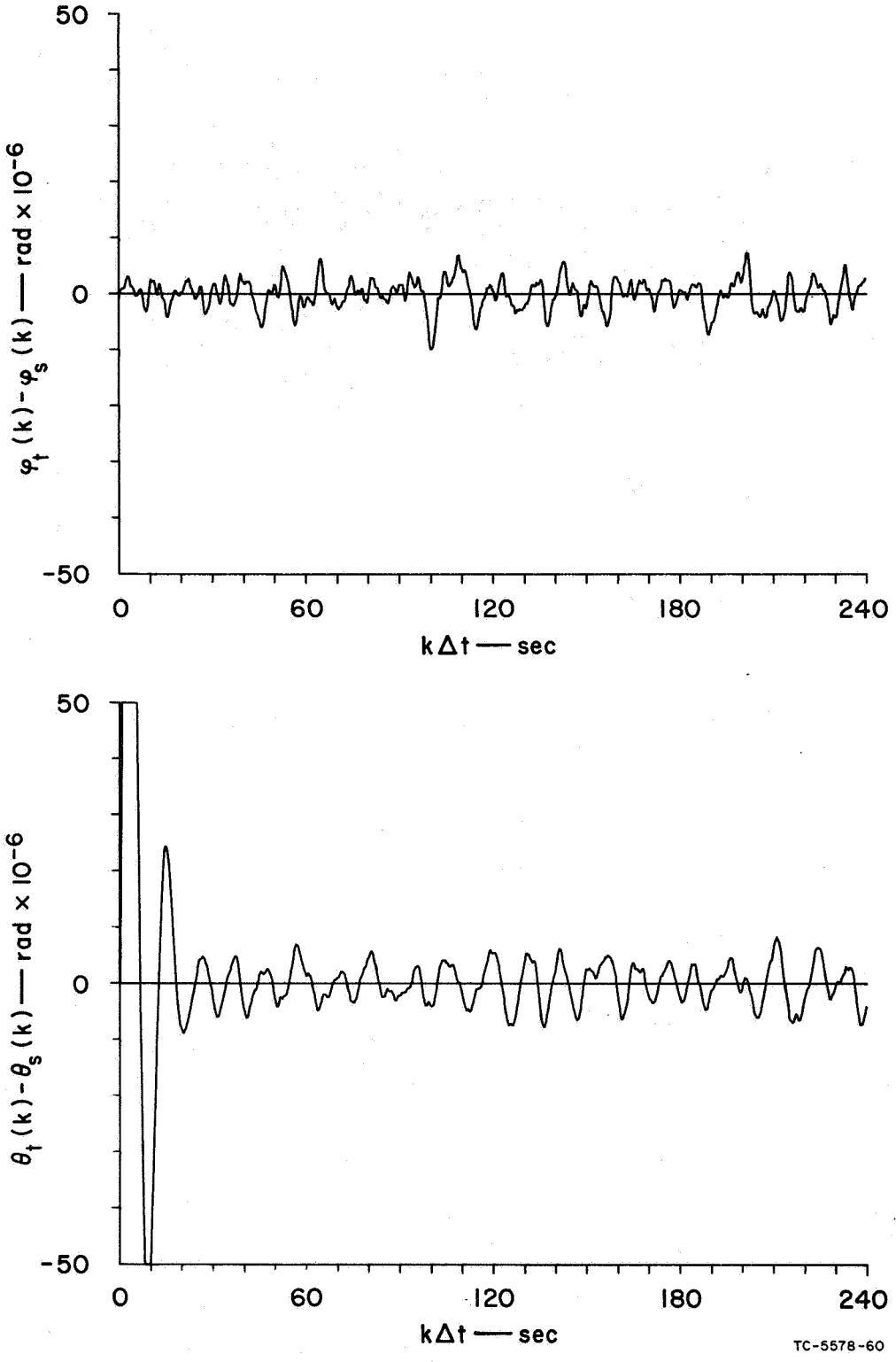

(b) TRACKING ERRORS

FIG. 17 Concluded

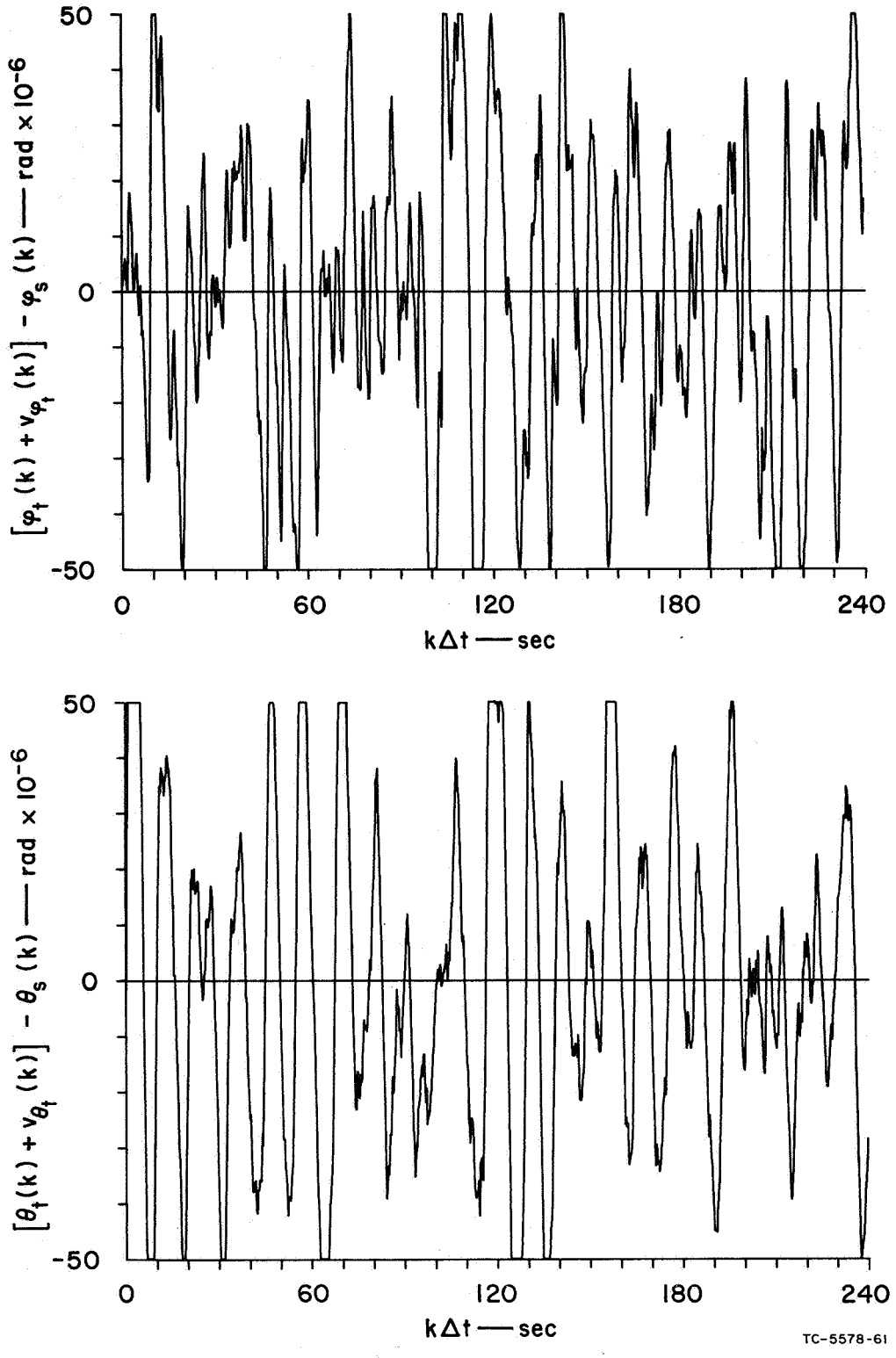

(a) ESTIMATION ERRORS

FIG. 18 AUTOTRACKER, $\sigma_{\varphi_a} = \sigma_{\theta_a} = 60 \times 10^{-6}$ rad, $\Delta t = 0.25$ sec

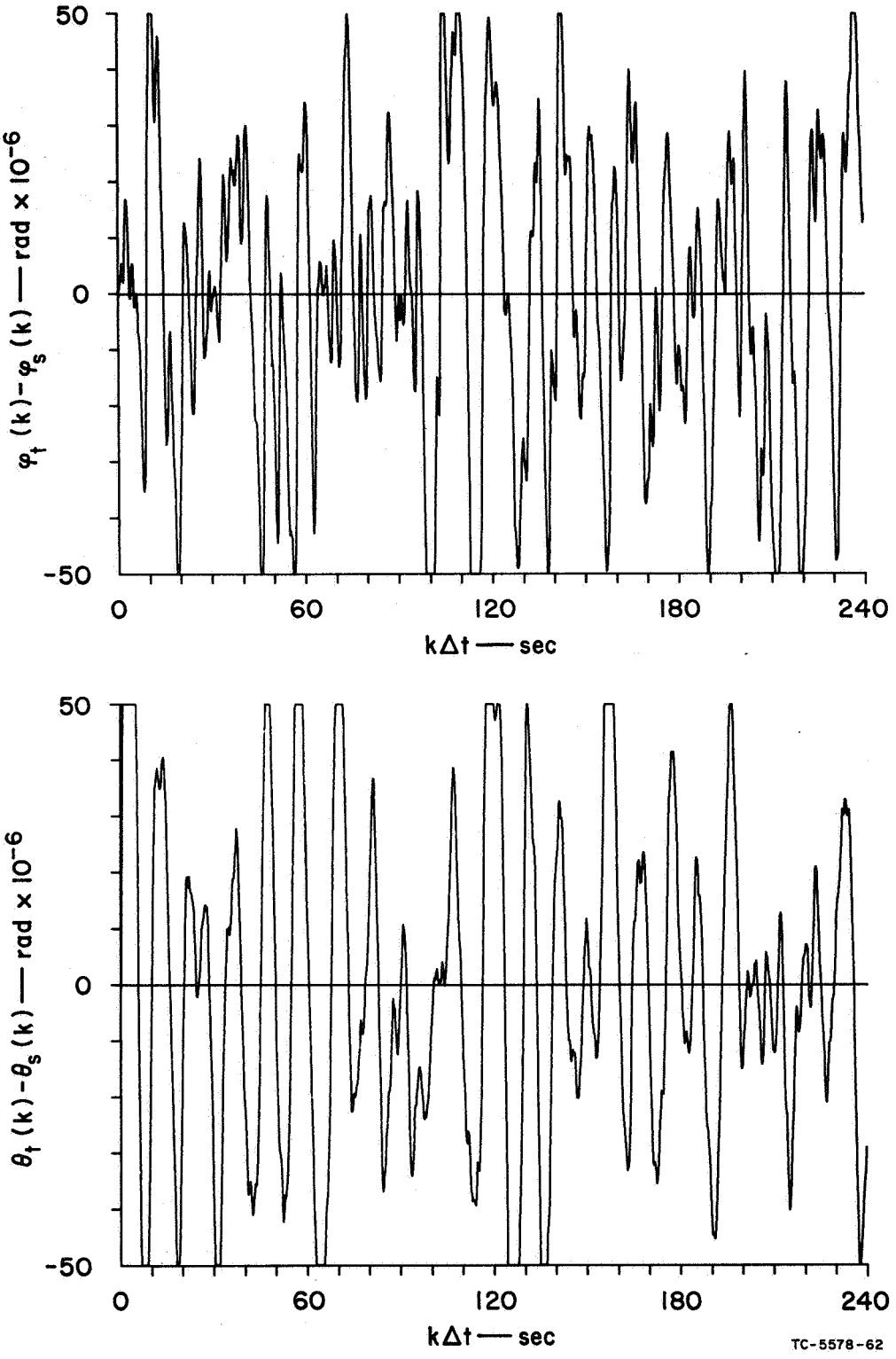

(b) TRACKING ERRORS

FIG. 18 Concluded

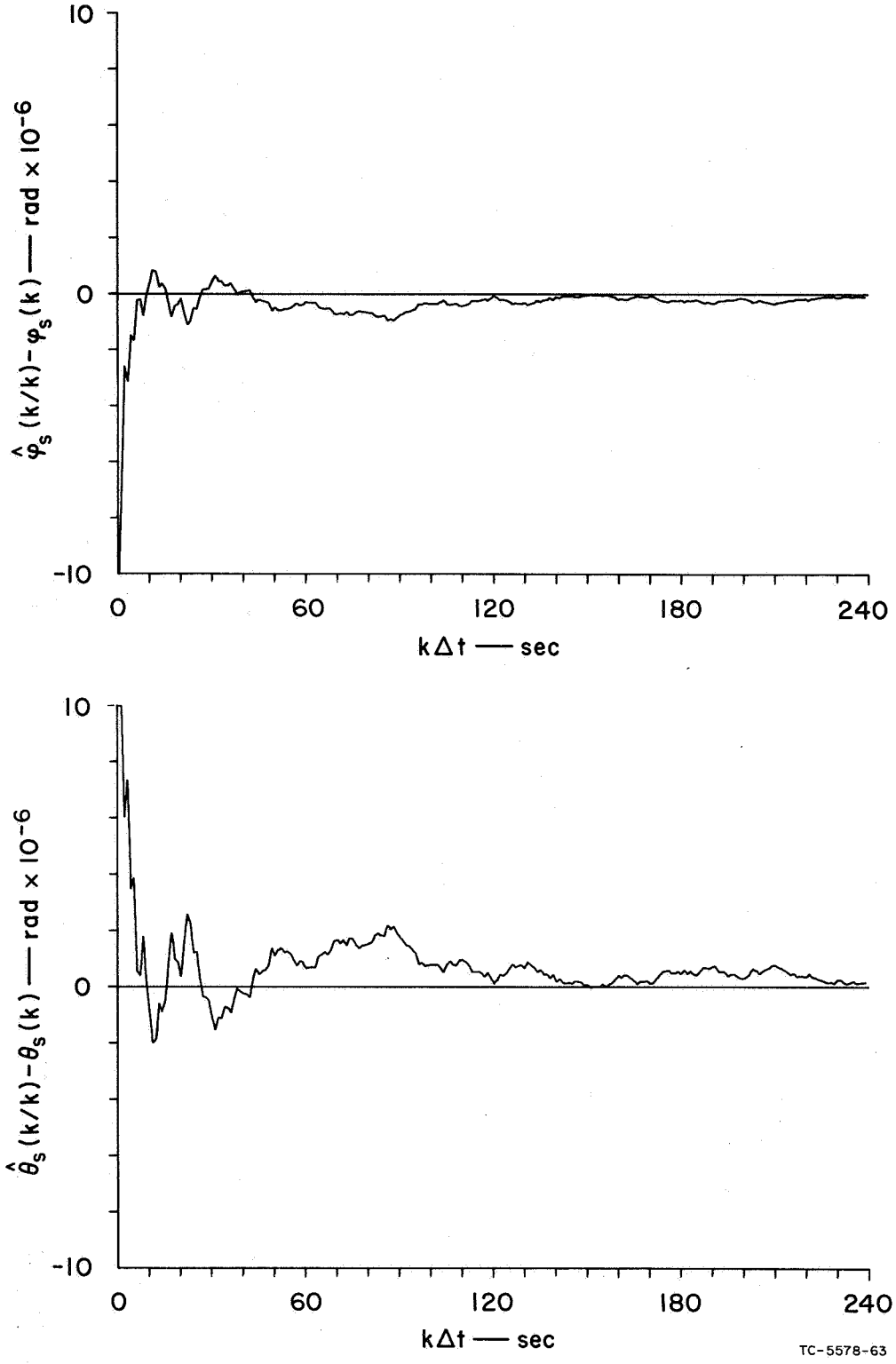

FIG. 19 ESTIMATOR–CONTROLLER (Case 1), $\sigma_{\varphi_a} = \sigma_{\theta_a} = 15 \times 10^{-6}$ rad, $\Delta t = 1.0$ sec

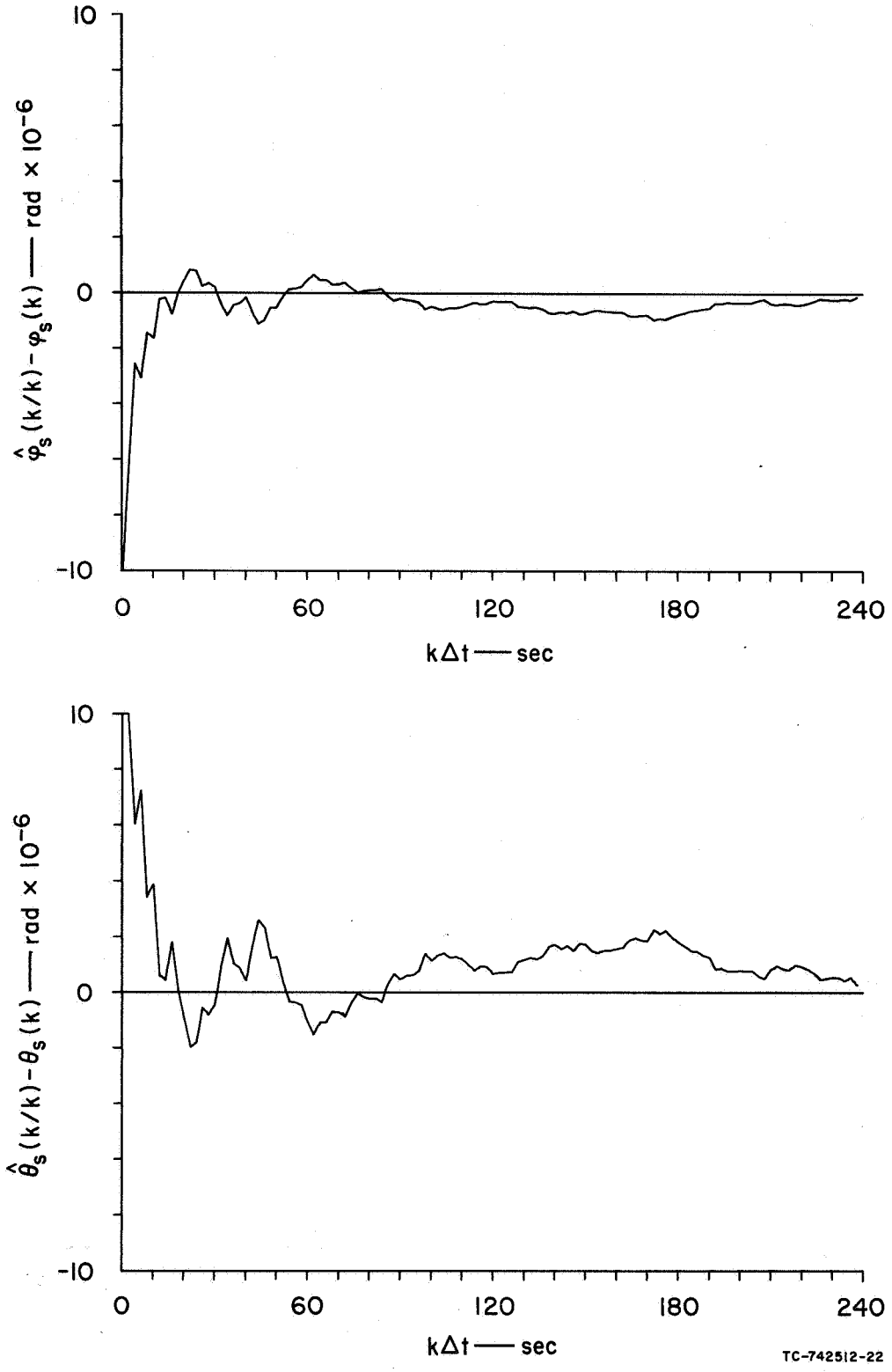

FIG. 20 ESTIMATOR–CONTROLLER (Case 1), $\sigma_{\varphi_a} = \sigma_{\theta_a} = 15 \times 10^{-6}$ rad, $\Delta t = 2.0$ sec

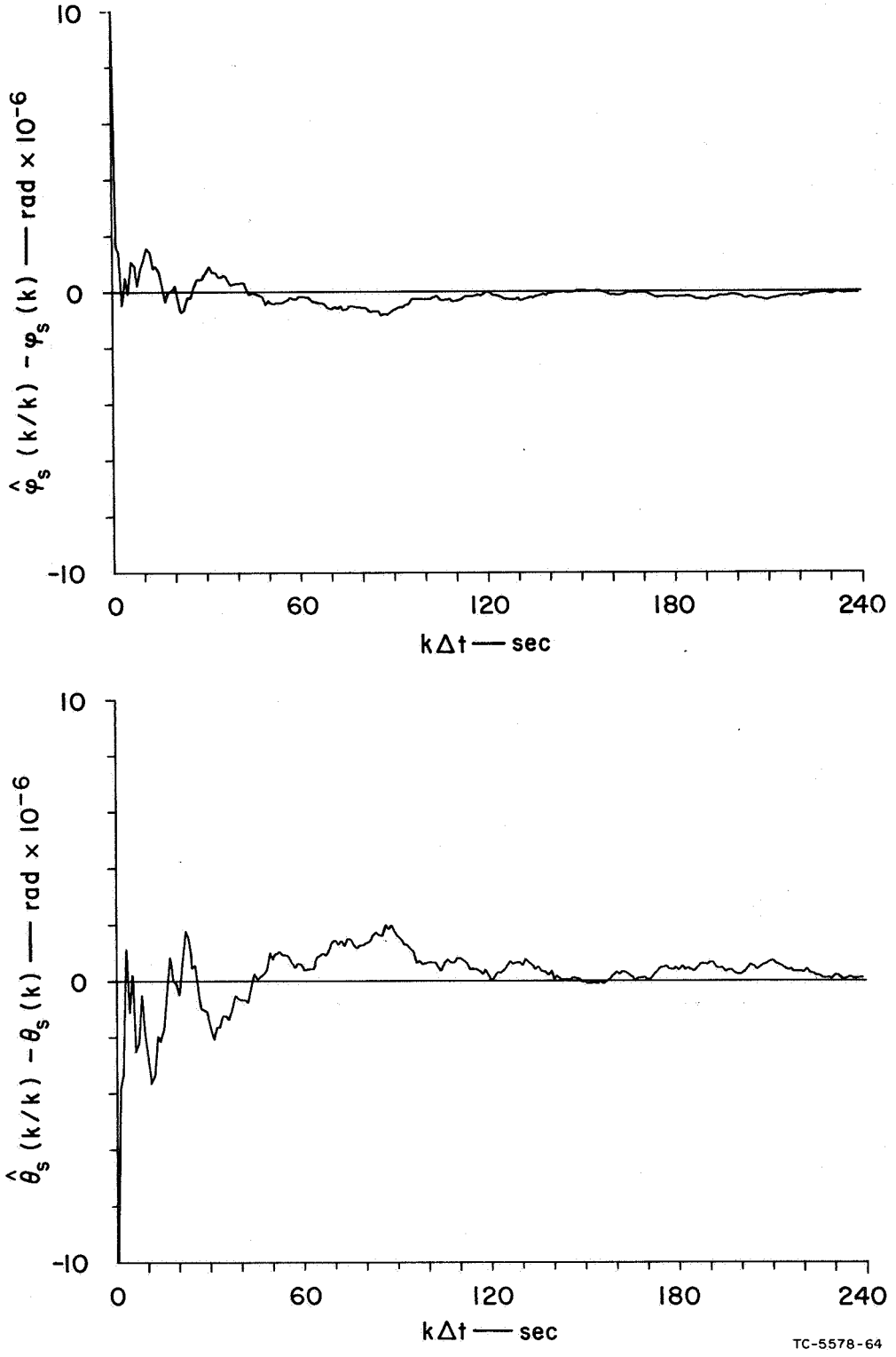

ESTIMATION ERRORS

FIG. 21 ESTIMATOR–CONTROLLER (Case 2), $\sigma_{\varphi_a} = \sigma_{\theta_a} = 15 \times 10^{-6}$ rad, $\Delta t = 1.0$ sec

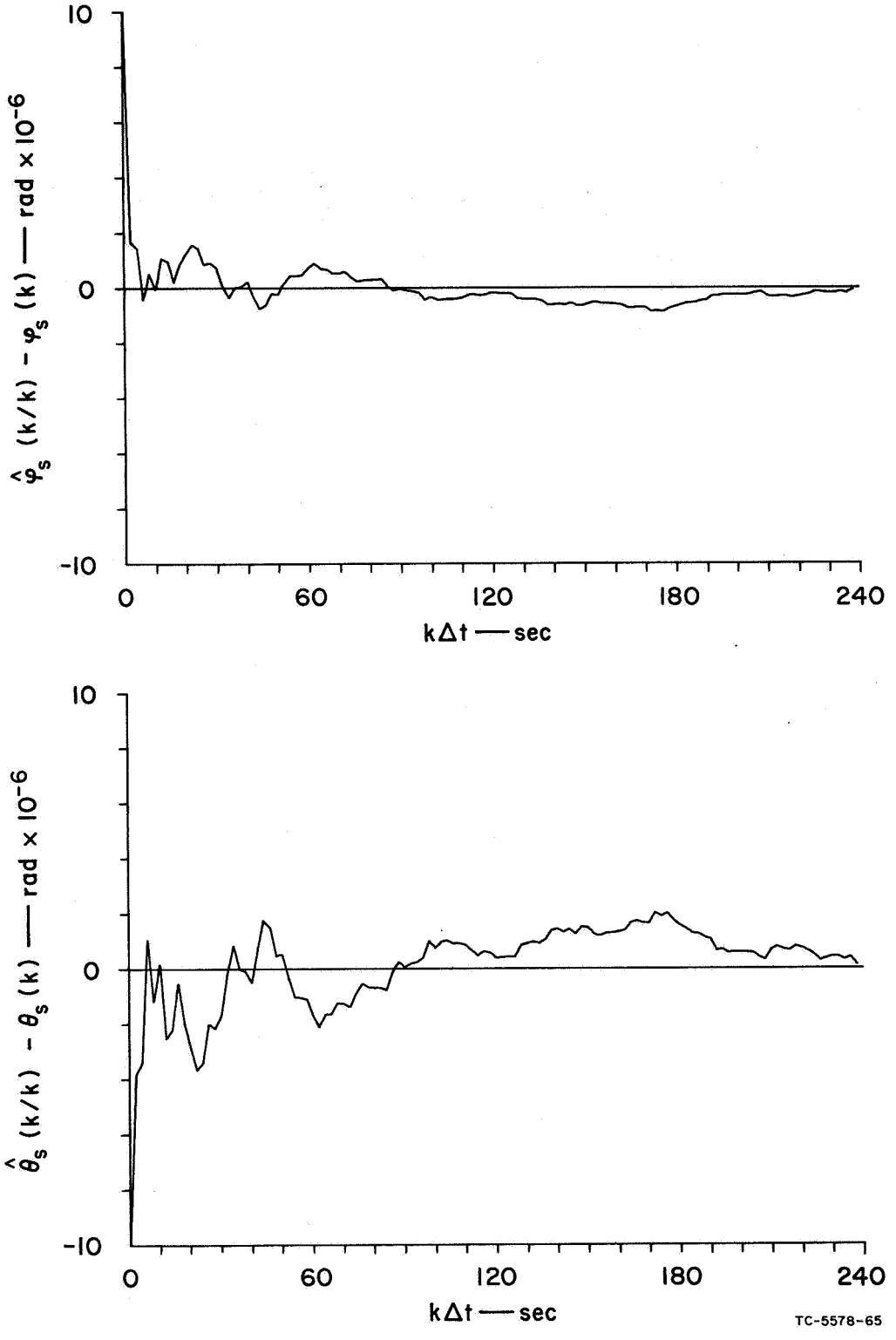

ESTIMATION ERRORS

FIG. 22 ESTIMATOR–CONTROLLER (Case 2), $\sigma_{\varphi_a} = \sigma_{\theta_a} = 15 \times 10^{-6}$rad, $\Delta t = 2.0$ sec

VI SUMMARY AND CONCLUSIONS

The research program described in this Final Report has investigated the control and tracking problems associated with an optical communication system operating between an earth station and a spacecraft assumed to be in the vicinity of Mars. The system performance specifications as well as the constraints imposed by the atmospheric and space propagation environment have been detailed, and their influences on the system design and performance limitations elaborated. Within this context several system design approaches were considered and the most promising, the cooperative configuration, chosen for detailed analysis. For this configuration, mathematical models of all system components were developed, including the relative motion of the two communication terminals, the dynamics of the earth-terminal receiving telescope, the optical propagation properties of the atmosphere and free space, and the noise characteristics of the optical and mechanical measuring devices used to obtain control or output data from the system.

Given this complete system specification, two design approaches were taken. The first, which results in the estimator-controller configuration developed in Sec. III, is based on results from optimal linear estimation and control theory. The principal feature of this theory is that the resultant systems can be shown to derive maximum benefit from the a priori design information, as well as information gathered during the system operation. The second control design is based on classical servo theory, which dictates that the resulting system exhibit zero steady-state tracking error and that the dynamic response of the system be specified so as to respond to the frequency spectrum of the signal while affording maximum rejection of the frequency spectrum of the noise and disturbances. The system developed by these techniques is termed an autotracker and is described in Sec. IV.

The optical communication and tracking system, employing either the estimator-controller or the autotracker, was simulated by means of

a digital computer so that comparative performance data could be obtained. Representative cases illustrating the performance obtained are shown in Sec. V. In addition to assessing the relative performance of the estimator-controller and autotracker, these simulation runs were also used to evaluate performance sensitivity to such parameters as the magnitude of atmospheric interference and iteration time for the computations.

On the basis of the results obtained during this research project, several general conclusions regarding the deep-space optical communication problem can be stated. First, and foremost, is the conclusion that it is within the capability of present technology to implement an optical communication system that will provide a significant increase in data rate over presently used techniques. Secondly, from the simulation test results shown in Sec. V, and given the assumption that the tracking system includes a high-speed beam steerer with a dynamic range of ±1 arc minute, it must be concluded that both the estimator-controller and the autotracker system designs are capable of maintaining continuous signal contact under the conditions simulated in the tests. This conclusion must, however, be viewed in the context of the assumptions that lead to it. The incorporation of a high-speed beam steerer in an optical system is not common practice in the design of large telescopes; therefore, in the event that such a device is not used, the field of view of the system must be made large enough to include both the anticipated atmospheric disturbances and the tracking errors. Under these circumstances the estimator-controller configuration, because of its smaller tracking errors (as shown in Sec. V) offers a definite advantage in that the field of view can be made smaller than for an autotracker system--thus permitting enhanced communication capacity. Furthermore, as was shown in Sec. V, the tracking error achieved by the estimator-controller configuration is much less sensitive to increases in the atmospheric disturbances than is that achieved by the autotracker; thus, the estimator-controller will be capable of maintaining successful system operation under more unfavorable atmospheric conditions than is possible with the autotracker.

Implicit in all of the discussions and simulations thus far has been the assumption that the tracking telescope is protected from its environment by a dome similar to that commonly used with astronomical telescopes. Such protection makes plausible the assumption that the telescope is not subject to stochastic torque disturbances from such sources as wind gusts. Disturbances of this type present the autotrack system designer with a dilemma. He would like to design a low bandwidth system to achieve good filtering of the signal being tracked; however, such a system will respond with large output excursions to load disturbance torques--quite likely in excess of the dynamic range of any beam steering mechanism employed. On the other hand, if the system bandwidth is made large enough to reduce the response to load disturbances to an acceptable level, then the filtering function is degraded and the system output will contain a large fraction of the noise corrupting the input signal. The resulting design is therefore a compromise between these two opposing factors. While there are many instances where such a compromise design may be adequate, it does not represent the optimum performance that can be achieved via modern design techniques.

In contrast, the estimator-controller approach is not faced with this dilemma since the tasks of filtering the noise-corrupted signals and of telescope control are accomplished separately. The estimator portion of the system is designed to produce the best possible estimates of spacecraft and telescope state and, thus, serves as a signal filter. The controller for the telescope is then operated as a position servo, following the outputs of the estimator. Since the controller is no longer called upon to perform a filtering function, the resulting system bandwidth can be made as large as necessary to adequately compensate for the load disturbances. Since the input to the controller has already been filtered by the estimator, the performance of the tracking system will not be degraded by this large bandwidth. Furthermore, the filtering of the input signals to the controller will eliminate those high frequency components that, although they are too high in frequency to directly affect the system output, could excite higher order

resonances within the mechanical and drive systems and thus degrade system performance.

In addition to maintaining uninterrupted contact between the two communication terminals, the tracking systems studied provide angle-tracking data on the spacecraft trajectory. At the extremely long ranges of a deep-space mission, it is questionable that the angle-tracking data will be competitive with that achievable by such existing tracking systems as range/range rate for ultimate accuracy in trajectory smoothing.

On the other hand, for near-earth vehicles and during the early phases of a deep-space mission, optical angle tracking will prove valuable for precise determinations of vehicle position and trajectory. Both the autotracker and the estimator-controller configurations can be employed to obtain this tracking data. As illustrated in Sec. V, the estimator-controller achieves appreciably smaller estimation errors than the autotracker. Subsequent processing of the autotrack data can reduce its inherent errors, but in those cases where real-time operation is required, as in vehicle guidance or trajectory determination for hand-off or interception, the estimator-controller configuration is capable of providing the best possible tracking data obtainable from the input information received up to that time.

The results of this research project, and the conclusions drawn from them, have established from theoretical considerations and simulations the feasibility and practicability of accomplishing tracking with an optical system to an unprecedented level of accuracy. The next logical step in the development of the concept of optical communication and tracking systems is the implementation, most likely at an existing optical facility, of an optical tracking system employing both a high-speed beam steerer and an estimator-controller system configuration. Experiments simulating the conditions of a deep-space optical communications mission conducted between such a facility and a cooperative satellite would serve to substantiate the conclusions drawn from the theoretical considerations. Furthermore, this same facility could

also be employed to evaluate optical tracking system capabilities as sources of tracking data for trajectory or orbit determination purposes.

REFERENCES

1. E. C. Fraser and R. M. Dressler, "Deep-Space Optical Communication Systems," Memorandum 8, Contract NAS12-59, SRI Project 5578, Stanford Research Institute, Menlo Park, California (30 December 1966).

2. "A System Study of a Manned Orbital Telescope," Report No. D2-84042-1, Contract NAS1-3968, Aerospace Group, The Boeing Company, Seattle, Washington (October 1965).

3. G. F. Bullock, "Scaling Techniques for a Vehicle-Control Simulation of a Proposed Manned Orbiting Telescope," Langley Working Paper LWP-360, NASA Langley Research Center, Hampton, Virginia (9 February 1967).

4. R. M. Dressler and E. C. Fraser, "Models for the Earth-Based Terminal of an Optical Communication System," Memorandum 9, Contract NAS12-59, SRI Project 5578, Stanford Research Institute, Menlo Park, California (March 1967).

5. G. P. Kuiper and B. M. Middlehurst, Telescopes (University of Chicago Press, Chicago, Illinois, 1960).

6. L. Meier, "Combined Optimum Control and Estimation Theory," Contractor Report, Contract NAS2-2457, SRI Project 5237, Stanford Research Institute, Menlo Park, California (October 1965).

7. R. E. Kalman, "A New Approach to Linear Filtering and Prediction Problems," Trans. ASME, J. Basic Engineering, pp. 35-45 (March 1960).

8. L. Meier, "Adaptive Control and the Combined Optimization Problem," Memorandum 6, Contract NAS12-59, SRI Project 5578, Stanford Research Institute, Menlo Park, California (10 February 1966).

9. R. E. Larson, R. M. Dressler, and J. Peschon, "Research on Adaptive Control System Design," Quarterly Report 3, Contract NAS12-59, SRI Project 5578, Stanford Research Institute, Menlo Park, California (April 1966).

10. G. C. Newton, L. A. Gould, and J. F. Kaiser, Analytical Design of Linear Feedback Controls (John Wiley & Sons, Inc., New York, New York, 1957).

11. J. M Stephenson, et al., "Design Criteria for a Large Multi-Purpose Tracking Antenna," WDL Tech. Rept. 1368, Philco Corp., Western Development Laboratories, Palo Alto, California (20 January 1961).

12. F. E. Nixon, Principles of Automatic Controls, (Prentice-Hall, Inc., Englewood Cliffs, New Jersey, 1953).

13. M. A. Kisner, "Earth-Based Terminal of the Optical Communication and Tracking System," Programmer's Manual, Contract NAS12-59, SRI Project 5578, Stanford Research Institute, Menlo Park, California (October 1967).

UNCLASSIFIED
Security Classification

DOCUMENT CONTROL DATA - R & D

(Security classification of title, body of abstract and indexing annotation must be entered when the overall report is classified)

1. ORIGINATING ACTIVITY *(Corporate author)* Stanford Research Institute 333 Ravenswood Avenue Menlo Park, California 94025	2a. REPORT SECURITY CLASSIFICATION Unclassified 2b. GROUP N/A

3. REPORT TITLE

OPTICAL COMMUNICATION AND TRACKING SYSTEMS

4. DESCRIPTIVE NOTES *(Type of report and inclusive dates)*
Final Report

5. AUTHOR(S) *(First name, middle initial, last name)*
Robert M. Dressler

Edward C. Fraser

6. REPORT DATE	7a. TOTAL NO. OF PAGES	7b. NO. OF REFS
October 1967	103	13

8a. CONTRACT OR GRANT NO.	9a. ORIGINATOR'S REPORT NUMBER(S)
NAS12-59 b. PROJECT NO.	SRI Project 5578 Final Report
c.	9b. OTHER REPORT NO(S) *(Any other numbers that may be assigned this report)*
d.	

10. DISTRIBUTION STATEMENT

11. SUPPLEMENTARY NOTES	12. SPONSORING MILITARY ACTIVITY
	National Aeronautics and Space Administration Electronics Research Center Cambridge, Massachusetts

13. ABSTRACT

The results of research performed by the Information and Control Laboratory of Stanford Research Institute for the Electronics Research Center of the National Aeronautics and Space Administration on Contract NAS12-59 from 1 October 1966 to 30 September 1967 are described in this Final Report. The research program has investigated the control and tracking problems associated with an optical communication system operating between the earth and a spacecraft in the vicinity of Mars. For the system configuration studied, mathematical models of all system components are developed including the relative motion of the two communication terminals, the dynamics of the earth-terminal receiving telescope, the optical propagation properties of the atmosphere and free space, and a statistical description of the optical and mechanical measuring devices used to obtain control or output data from the system.

Two design approaches to this problem are taken. The first, which is based on results from optimal linear estimation and control theory, results in the estimator-controller configuration. The second design employs classical servo theory and yields the autotracker system. The optical communication and tracking system, employing either the estimator-controller or the autotracker, was simulated by means of a digital computer. In addition to assessing the relative performance of these two system designs, computer simulations were also used to evaluate performance sensitivity to such parameters as the magnitude of atmospheric interference and iteration time for the computations.

DD FORM 1473

13. ABSTRACT (Continued)

The simulation tests demonstrate that although, for nominal environmental conditions, both the estimator-controller and the autotracker perform satisfactorily, the estimator-controller is able to maintain satisfactory performance under conditions that render the autotracker unusable.

On the basis of results obtained during this research project, it can be concluded that it is within the capability of present technology to implement a deep-space optical communication system that will provide a significant increase in data rate over presently used techniques.

14. KEY WORDS	LINK A		LINK B		LINK C	
	ROLE	WT	ROLE	WT	ROLE	WT
Optical Communication and Tracking System						
Linear Optimal Estimation and Control Theory						
Optical Error Detector						
Computer Simulation						
Deep-Space Communication						